hydrology

MDPI

Article

Integrated Multi-Evidence Modeling of River–Groundwater Interactions and Sustainable Water Use in the Arid Aksu River Basin, Northwest China

Jingya Ban [1,2,*], Shukun Ni [1,2], Zhilin Bao [1,2], Bin Wu [1,2] and Chuanhong Ye [1,2]

[1] College of Hydraulic and Civil Engineering, Xinjiang Agricultural University, Urumqi 830052, China; 15029238122@163.com (S.N.); baozhilin835@163.com (Z.B.); wubinxj@163.com (B.W.); 17302356740@163.com (C.Y.)
[2] Xinjiang Key Laboratory of Hydraulic Engineering Security and Water Disasters Prevention, Urumqi 830052, China
* Correspondence: banjingya@xjau.edu.cn

Abstract

The Aksu River Basin, the main headwater of the Tarim River, contributes more than 70% of the main stream's runoff and is therefore critical in maintaining hydrological stability in this arid river system. In recent decades, rapid oasis expansion and growing agricultural water withdrawals have intensified competition for surface and groundwater, posing increasing ecological risks to the downstream Tarim River Basin. To quantitatively characterize river–groundwater hydrological responses under intensive water use, we combined statistical analysis, field observations, and distributed hydrological modeling within a basin-scale conceptual framework. Multiple lines of evidence—water level monitoring, hydrochemical tracers, stable isotopes, and the integrated surface–groundwater model MIKE SHE—were used to identify river–groundwater interaction mechanisms in the Aksu alluvial plain. Results reveal a typical three-stage spatial exchange pattern: river recharge to groundwater in the upstream reach, groundwater discharge to the river in the midstream, and renewed river infiltration to groundwater downstream. The patterns inferred from water levels, hydrochemistry, and isotopes are broadly consistent, while water-level data better resolve left–right bank asymmetry. The MIKE SHE model supports the seasonal bidirectional exchange dynamics and reproduces runoff behavior with acceptable performance (RMSE and residual standard deviation within 20% of observed means and $R^2 > 0.7$ during both calibration (2010–2017) and validation (2018–2021)). The proposed multi-evidence framework captures the spatio-temporal variability of river–groundwater interactions in arid regions and provides spatially differentiated guidance for conjunctive surface–groundwater regulation and integrated water resources management in the Tarim River Basin.

Keywords: arid region; Aksu River Basin; river–groundwater interaction; MIKE SHE model; integrated water resources management

Check for updates

Academic Editor: Marco Delle Rose

Received: 14 February 2026
Revised: 6 March 2026
Accepted: 7 March 2026
Published: 16 March 2026

Copyright: © 2026 by the authors. Licensee MDPI, Basel, Switzerland. This article is an open access article distributed under the terms and conditions of the Creative Commons Attribution (CC BY) license.

1. Introduction

Groundwater constitutes a major component of the Earth's liquid freshwater, accounting for approximately 98.5% of the total freshwater resources, and plays a crucial role in social, economic, and ecological systems. In arid and semi-arid regions, precipitation is scarce and surface water is often insufficient during low-flow periods, whereas groundwater—due to its relatively stable recharge—is regarded as an indispensable water

source [1]. The interaction between surface water and groundwater represents a core component of the hydrological cycle; its dynamic relationship not only governs the balance between runoff and groundwater levels but also directly determines the sustainability of regional water resources management [2]. In recent years, river–groundwater interaction interactions have become a major research focus, particularly with respect to the disconnection processes of intermittent rivers and their driving mechanisms [3]. Current approaches for investigating river–groundwater interactions can be broadly classified into three categories: (1) flux-based methods, such as cross-sectional flow measurement [4], water balance analysis [5], and baseflow separation [6], which enable quantitative characterization of exchanges but are difficult to apply over long time periods or large spatial scales; (2) environmental tracer methods, including hydrochemistry, stable isotopes [7], and temperature tracing [8], which are simple and effective but often subject to spatial disturbances and high monitoring costs; (3) mathematical modeling approaches, which have gained increasing popularity with advances in remote sensing and big data technologies. Since Lloyd first conducted numerical simulations in desert regions [9], a variety of distributed and coupled models have been developed and applied to quantify recharge processes, river–groundwater interaction exchanges, and hydro-salinity evolution under arid conditions [10–14]. Domestic studies, which began relatively late during the 1980s and 1990s [15,16], have gradually shifted from regional water balance analysis toward mechanism-oriented modeling and integrated simulation since the beginning of the 21st century [17–20].

Distributed hydrological models have been widely applied because they can effectively represent the spatial heterogeneity of underlying surfaces [21–23]. Numerical models such as the Soil and Water Assessment Tool (SWAT), the Variable Infiltration Capacity (VIC) model, MODFLOW, and FEFLOW, along with modeling environments like the Groundwater Modeling System (GMS), have been extensively used in arid basins to simulate runoff generation, groundwater flow, and surface–subsurface interactions [24–30]. To overcome the limitations of single models, multi-model coupling approaches and fully integrated platforms, such as SWAT–MODFLOW, MIKE SHE, and HydroGeoSphere, have demonstrated improved capability in reproducing coupled hydrological processes [31–38]. In parallel, data-driven approaches based on machine learning and deep learning (e.g., XGBoost, RNN, and LSTM) have shown promising performance in runoff prediction [39], although their limited physical interpretability and risk of overfitting remain important concerns [40]. In recent years, the impact of groundwater abstraction on watershed runoff patterns has gradually become a key research focus. Rivers in arid regions mainly rely on mountain precipitation, snow and ice melt, and groundwater recharge [41]. However, as groundwater levels decline, the balance of water flow, sediment, and salinity within the basin becomes disturbed, thereby aggravating water scarcity and ecological degradation [42]. Declining groundwater levels constrain irrigation supply and may exacerbate salinization, posing serious threats to agricultural production and ecosystem stability [43–46]. Existing studies have demonstrated that excessive groundwater withdrawal reduces water storage, disrupts the equilibrium between groundwater and river exchange, and consequently alters runoff processes and hydrological regimes [47–50].

In summary, although considerable progress has been made both domestically and internationally in understanding river–groundwater interactions and hydrological cycle modeling, several important limitations remain. First, although many previous investigations combine hydrochemical analyses, isotopic tracing, and groundwater level observations, these multiple lines of evidence are often applied in a loosely coupled manner, lacking highly coordinated and system-level integration across spatial and temporal scales. Second, insufficient attention has been paid to the explicit incorporation of human activities,

particularly oasis expansion and agricultural water withdrawals, within physically based coupled modeling frameworks. Third, model applications are frequently constrained by limited calibration and validation data, and scenario-based forecasting for future water resource utilization remains relatively scarce. Therefore, it is imperative to develop hydrological modeling frameworks tailored to arid inland basins that integrate multiple observational datasets in a coordinated manner and explicitly represent human-induced hydrological disturbances. Based on these considerations, this study selects the Aksu River Basin as a representative case and integrates multiple observational datasets, including hydrochemical analyses, stable isotope tracing, groundwater-level observations, and physically based numerical modeling, within a unified and coordinated multi-dataset framework to systematically elucidate river–groundwater transformation mechanisms. The objectives of this study are to (1) clarify the spatial recharge–discharge patterns between rivers and groundwater in plain areas, (2) enhance the reliability of mechanism interpretation through coordinated cross-validation of multiple datasets, and (3) provide scientific guidance for water resource management under different groundwater exploitation scenarios.

2. Study Area and Data Sources

2.1. Overview of the Study Area

The Aksu River Basin is located in the central southern foothills of the Tianshan Mountains and the northwestern margin of the Tarim Basin, Xinjiang Uygur Autonomous Region, China. It serves as a key hub of the "Silk Road Economic Belt" and represents the largest river basin in southern Xinjiang. The basin covers a total area of 3.49×10^4 km^2, including a plain area of 1.4×10^4 km^2 and a mountainous–hilly area of 2.09×10^4 km^2, encompassing five administrative divisions: Aksu City, Wensu County, Wushi County, Awat County, and Keping County [51]. The basin experiences a typical warm temperate continental arid climate, characterized by scarce precipitation concentrated in the summer and potential evaporation far exceeding rainfall. The minimum winter temperature can drop to −20 °C, while the maximum summer temperature exceeds 40 °C, accompanied by large diurnal temperature variations. In spring, frequent strong winds and dust storms further intensify soil moisture evaporation. The mountainous region is relatively humid, forming a distinct climatic contrast with the plains and desert areas [52,53]. The Aksu River is the largest tributary and the primary source of recharge for the Tarim River. From 1960 to 2018, its multi-year average inflow was 8.308×10^9 m^3, accounting for approximately 74% of the main stream's runoff. The main river channel extends for 132 km, from the Xidaqiao station to the Yimanpaxia sluice, with a multi-year average runoff of 6.567×10^9 m^3 during 1960–2022 [54]. At Ailishi, the river bifurcates into the Xindah River (59%) and the Laodah River (41%), which eventually converge into the Tarim River at Xiaojiake. As the only tributary that continuously supplies the main stream, the Aksu River contributes 70–80% of the annual inflow. Although the overall supply is stable, its seasonal variation is pronounced: spring accounts for only 7.02–9.90%, while summer reaches as high as 58.7–68.6%, with the maximum in July and the minimum in February, exhibiting the typical pattern of "spring drought, summer flood, autumn scarcity, and winter depletion" [55,56]. In summary, the Aksu River Basin exhibits highly representative natural geographic and climatic characteristics. Its water resources not only sustain oasis agriculture and downstream ecological security but also play a vital role in regional sustainable development and national strategic stability. Figure 1 presents an overview of the study area.

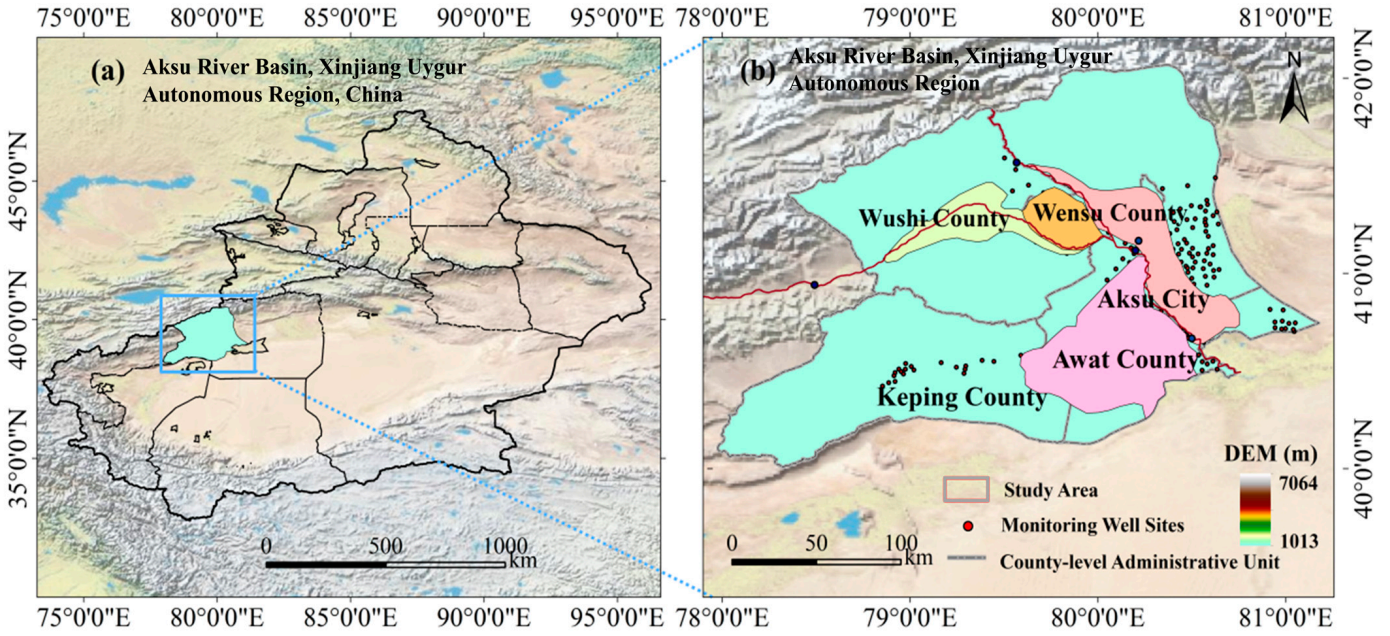

Figure 1. Location and overview map of the study area: (**a**) regional location of the Aksu River Basin in Xinjiang Uygur Autonomous Region, China; (**b**) enlarged map of the study area showing the county-level administrative units, the study area (rectangle), and the monitoring station (dot).

2.2. Data Source and Processing

The data used in this study integrate multi-source observations and remote sensing datasets, providing a solid foundation for the comprehensive analysis and numerical simulation of river–groundwater interaction in the Aksu River Basin.

The remote sensing and land-use data include the basin boundary (from the National Geoinformation Service Platform, https://www.tianditu.gov.cn (accessed on 15 March 2025)), land-use status (from the Data Center for Resources and Environmental Sciences, Chinese Academy of Sciences, https://www.resdc.cn/Default.aspx (accessed on 15 March 2025)), soil type (from the World Soil Database, https://www.fao.org/soils-portal/en (accessed on 15 March 2025)), and vegetation parameters (from the FAO database, https://www.fao.org/faostat/en/home (accessed on 15 March 2025)), which were used for spatial parameterization and irrigation process simulation in the MIKE SHE model.

Meteorological data, including precipitation and potential evapotranspiration, were obtained from the China Meteorological Data Service Center (https://data.cma.cn (accessed on 15 March 2025)) to drive precipitation–evapotranspiration balance processes in the model. During data preprocessing, missing values in runoff and groundwater-level time series were interpolated, outliers were removed, and trends were smoothed to enhance temporal continuity and stability. Spatial consistency across meteorological, hydrological, and remote sensing datasets was achieved by unifying them under the WGS_1984 coordinate system and standardizing their resolutions. Additionally, laboratory-based standardization and quality control were applied to hydrochemical and isotopic data to ensure comparability and consistency across both temporal and spatial dimensions. Ultimately, a comprehensive MIKE SHE model database integrating DEM, soil, land use, and meteorological datasets was established, providing a reliable foundation for the multi-evidence analysis and scenario-based simulation of river–groundwater interactions in the Aksu River Basin.

3. Research Methods

3.1. Water Level Analysis Method

The study was conducted in the alluvial plain reach of the lower Aksu River, where river water and shallow groundwater are hydraulically connected. River–groundwater exchange direction was inferred from the sign of the hydraulic head difference (groundwater head minus river stage), with groundwater discharge to the river when groundwater head exceeded river stage, and river leakage to the aquifer when river stage exceeded groundwater head [57–59]. To quantify longitudinal and lateral head gradients, eight monitoring cross-sections were established along an ~150 km reach from the Xiehela hydrological station to the Xidaqiao and Yimanpaxia sluices (Figure 2), with an average spacing of ~20 km. At each cross-section, river stage was measured within the channel, and 3–5 groundwater observation wells were installed on both banks within 3 km of the river, yielding 37 monitoring sites in total (Figure 3). Additional points were added at selected cross-sections where bank profiles were markedly asymmetric to better capture lateral head gradients.

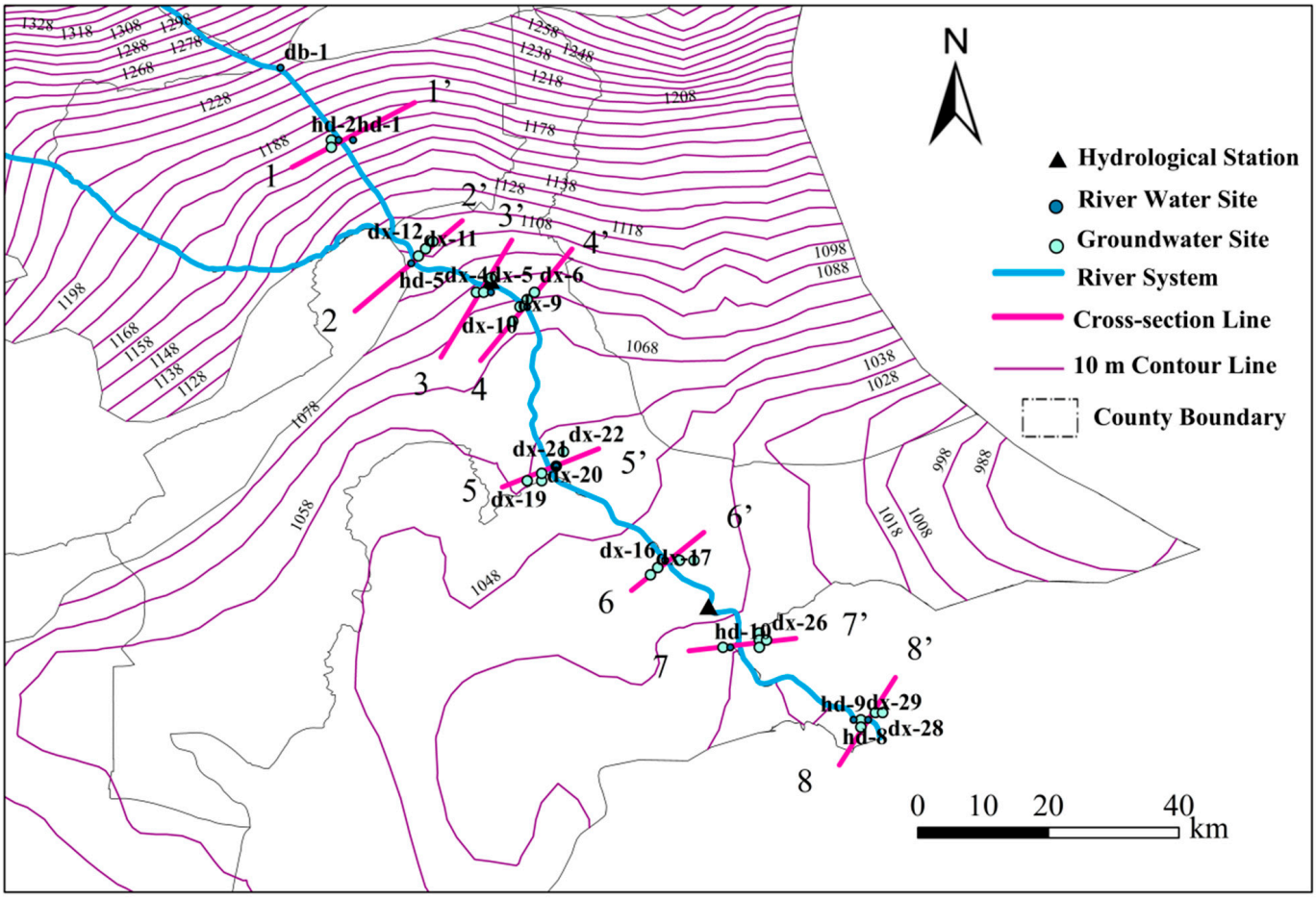

Figure 2. Location of the eight monitoring cross-sections along the lower Aksu River between Xidaqiao and Yimanpaxia.

Monitoring was conducted during the high-temperature season, when the dry–wet transition is pronounced and river recharge, evapotranspiration, and groundwater abstraction jointly influence river–groundwater interaction head dynamics.

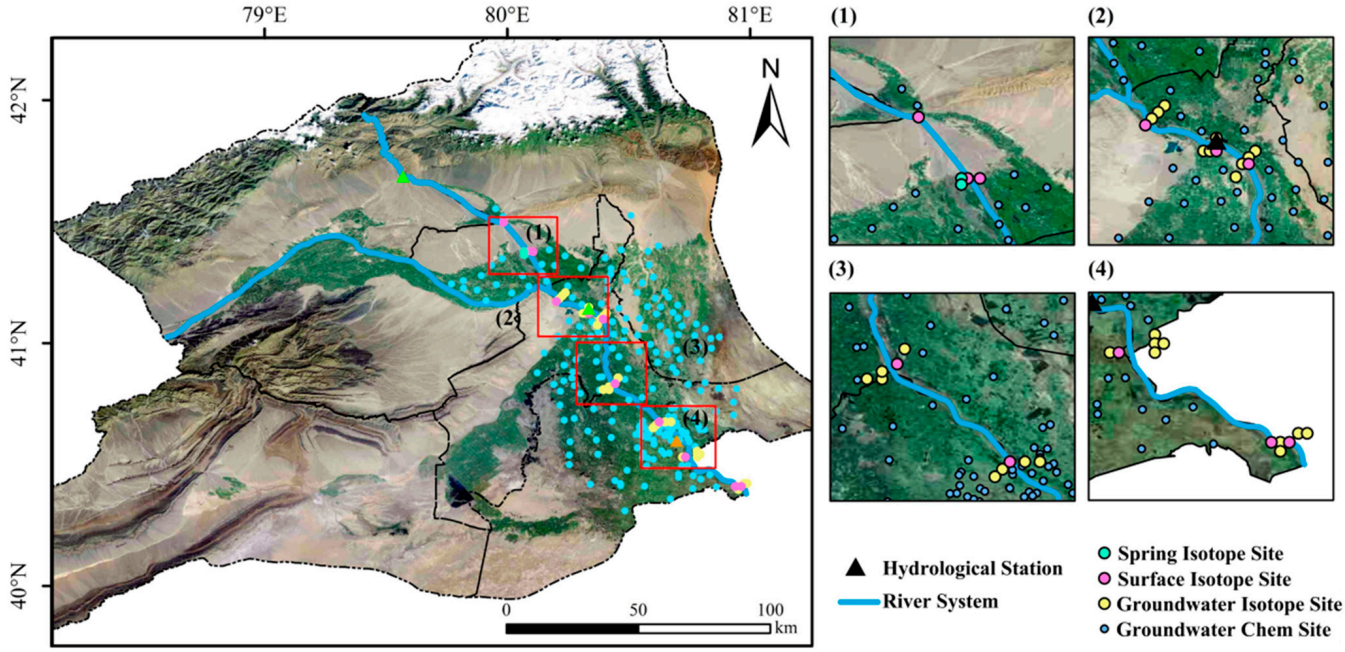

Figure 3. Schematic diagram of sample collection in the Aksu River Basin, showing the distribution of hydrological stations, river systems, county boundaries, and sampling sites for spring water, surface water, groundwater isotopes, and groundwater chemistry. Red boxes indicate the enlarged areas shown in panels (1)–(4).

3.2. Hydrochemical Characterization Method

Groundwater hydrochemical sampling was designed to ensure broad spatial coverage across the basin while representing the shallow aquifer system that is hydraulically connected to the Aksu River. In June 2023, groundwater samples were collected from 305 operational irrigation wells distributed throughout the study area using a uniform spatial sampling scheme. These wells are screened within the shallow aquifer composed primarily of Quaternary alluvial and fluvial deposits consisting of unconsolidated sand, gravel, and silty sediments, which form the principal groundwater-bearing units in the basin. This shallow aquifer system is the primary source of irrigation water and is hydraulically responsive to river–groundwater interactions. Groundwater depths (water levels) were measured simultaneously at each site using a water-level tape to ensure consistency between hydrochemical and hydraulic datasets.

Prior to sampling, groundwater was pumped sufficiently to remove stagnant water and obtain representative aquifer water. Duplicate groundwater samples were collected in pre-cleaned 250 mL high-density polyethylene (HDPE) bottles. Site coordinates, well locations, and field observations were recorded concurrently to ensure spatial consistency and traceability of the sampling network.

To support detailed comparisons between river water and groundwater along the monitored river reach, supplementary sampling was conducted in July 2024 along eight representative cross-sections between Xidaqiao and Yimanpaxia (Section 3.1). This campaign included 11 river-water samples, 28 groundwater samples, and 2 spring-water samples. River-water samples were collected from gently flowing sections of the main channel, avoiding stagnant marginal zones to ensure representative flow conditions. Samples were obtained using a bailer sampler and stored in 100 mL HDPE bottles after repeated rinsing with sample water. All bottles were filled completely without headspace, sealed with Parafilm, and stored under cold, dark conditions prior to laboratory analysis.

Groundwater samples associated with each cross-section were collected from wells and boreholes located within approximately 2 km of the river channel on both riverbanks, with

sampling intervals of approximately 500 m where feasible. These wells primarily tap the shallow alluvial aquifer that is hydraulically connected to the river system. High-precision geographic coordinates and elevations of all sampling locations were determined using Real-Time Kinematic Global Navigation Satellite System (RTK GNSS) positioning, which provides centimeter-level spatial accuracy. This high positional precision ensured reliable spatial alignment between river-water and groundwater sampling points and allowed accurate comparison of river stage and groundwater levels. River stage and groundwater depths were measured simultaneously to ensure spatial comparability and consistency in hydraulic interpretation across cross-sections.

Laboratory analyses included major ions, total dissolved solids (TDS), electrical conductivity (EC), and pH. Major anions (SO_4^{2-}, Cl^-, HCO_3^-, NO_3^-, Br^-) were measured using ion chromatography (CIC-D120), while major cations (Mg^{2+}, Ca^{2+}, Na^+, and K^+) were determined using inductively coupled plasma optical emission spectrometry (ICP-OES). The method detection limits ranged from 0.0018 to 0.007 mg/L for anions and from 0.002 to 0.007 mg/L for cations, and the corresponding limits of quantification were defined as three times the detection limits. Analytical quality was assessed using charge-balance errors, which were generally within ±5%, indicating high analytical reliability.

All sample collection, preservation, and laboratory procedures followed the Technical Specification for Groundwater Environmental Monitoring (HL/T164-2004), ensuring consistency with national groundwater monitoring standards.

3.3. Stable Isotope Analysis Method

Stable isotopes ($\delta^2H/\delta D$ and $\delta^{18}O$) were used to diagnose evaporation signals and river–groundwater exchange along the monitored Aksu River reach. Because long-term local precipitation isotope observations were unavailable, precipitation isotope characteristics were constrained using the Global Network of Isotopes in Precipitation (GNIP) dataset and interpreted with reference to the Global Meteoric Water Line (GMWL: $\delta D = 8\delta^{18}O + 10$). Deviations of surface water and groundwater isotope compositions from the meteoric water line were used to infer evaporative enrichment and recharge–discharge relationships.

River water, groundwater, and spring water isotope samples were collected along the eight monitoring cross-sections described in Sections 3.1 and 3.2. The spatial (longitudinal) variations in mean δD and $\delta^{18}O$ values were analyzed to characterize exchange processes and isotopic gradients between river water and groundwater [60–62].

For quantitative source apportionment, the MixSIAR Bayesian mixing model implemented in R was applied using δD and $\delta^{18}O$ as tracers. Precipitation/ice–snow meltwater, river water, and groundwater were defined as end-members to estimate recharge proportions at each cross-section. The model outputs posterior distributions for each end-member contribution, from which mean estimates and uncertainty intervals were reported.

Isotopic measurements were performed at Beijing TST Testing Technology Laboratory using a Picarro L2140-i liquid water isotope analyzer (Picarro, Inc., Santa Clara, CA, USA) based on cavity ring-down spectroscopy (CRDS). Samples were filtered through 0.22 μm membranes and stored in 2 mL vials. Each sample was measured six times, and the mean of the last three injections was adopted. Calibration was conducted using international water standards (GWB04458, GWB04459, and GWB04460). The analytical precision was $\delta^{18}O \pm 0.2‰$ and δD (δ^2H) ± 0.5‰, meeting the requirements of this study.

The isotope results were expressed in per mil (‰) relative to Vienna Standard Mean Ocean Water (V-SMOW):

$$\delta^{18}O = \left(\frac{R_{\text{O-sample}}}{R_{\text{V-SMOW}}} - 1\right) \times 1000\% \quad (1)$$

$$\delta D = \left(\frac{R_{\text{D-sample}}}{R_{\text{V-SMOW}}} - 1 \right) \times 1000\% \quad (2)$$

where $R_{\text{D-sample}}$ represents the D/H ratio of the water sample, $R_{\text{O-sample}}$ represents the $^{18}O/^{16}O$ ratio of the water sample, and $R_{\text{V-SMOW}}$ represents the D/H or $^{18}O/^{16}O$ ratio in Vienna Standard Mean Ocean Water (V-SMOW).

3.4. MIKE SHE Numerical Modeling Method

MIKE SHE is a fully distributed, physically based integrated hydrological modeling system designed to simulate the coupled processes of surface water and groundwater within a unified framework. In this study, a coupled MIKE SHE–MIKE 11 modeling system was developed for the Aksu River reach between Xidaqiao and Yimanpaxia to quantitatively characterize river–groundwater interactions at the watershed scale [63].

3.4.1. Model Structure

The modeling framework consists of several interacting components, including the overland flow module, unsaturated zone module, saturated groundwater module, and the river channel module dynamically coupled with MIKE 11. Surface processes, including rainfall interception, soil evaporation, and plant transpiration, were simulated using the Kristensen–Jensen evapotranspiration formulation based on vegetation parameters such as leaf area index and rooting depth. Overland flow generation and routing were represented using a two-dimensional diffusion-wave approximation parameterized by Manning's roughness coefficients.

The unsaturated zone was simulated using a one-dimensional vertical flow formulation based on the Richards equation to describe soil water redistribution and groundwater recharge, with soil hydraulic parameters derived from soil texture data. Groundwater flow in the saturated zone was represented using a three-dimensional finite-difference formulation of Darcy's law, assuming a heterogeneous but isotropic aquifer system. River flow dynamics were simulated using MIKE 11 based on the one-dimensional Saint-Venant equations. Dynamic coupling between MIKE SHE and MIKE 11 enabled two-way exchange between river water levels and groundwater heads, allowing explicit simulation of river leakage, groundwater discharge to the river, and channel evaporation losses. A detailed description of the governing equations can be found in the MIKE SHE documentation [64–68].

3.4.2. Boundary Conditions and Spatial Discretization

The model domain covers approximately 3.49×10^4 km^2 and was discretized using a regular grid with a horizontal resolution of 1 km, resulting in 34,909 computational cells. The original 30 m digital elevation model was resampled to 1 km to balance the representation of major topographic gradients and computational efficiency. All spatial datasets were projected to the WGS_1984_UTM_Zone_44N coordinate system and converted into MIKE SHE input formats.

Upstream river boundaries were specified using observed daily streamflow at two hydrological stations, while downstream boundaries were defined using observed water levels. Lateral groundwater boundaries were treated as no-flow (zero-flux) conditions, assuming negligible regional groundwater inflow or outflow across the basin margins. Meteorological forcing data (precipitation, air temperature, and reference evapotranspiration) for the period 2010–2021 were derived from daily station observations and spatially interpolated to the model grid using a combination of Thiessen polygon regionalization and Kriging interpolation [69].

3.4.3. Parameterization, Calibration, and Validation

Model parameters were derived from multiple data sources, including a 30 m land-use dataset, soil texture data from the World Soil Database, and regional hydrogeological maps provided by the China Geological Survey. Soil hydraulic parameters were estimated using RETC software 6.02, and vegetation parameters were assigned according to land-use classes and growth stages. Aquifer hydraulic conductivities and storage parameters were initially defined based on regional geological information and subsequently refined during model calibration.

Model calibration was performed using daily streamflow observations at the Xidaqiao and Yimanpaxia stations for the period 2010–2017, and model performance was validated for the period 2018–2021. Model performance was evaluated using the coefficient of determination (R^2), root mean square error (RMSE), and the standard deviation of residuals. For both stations, R^2 values exceeded 0.84 during both calibration and validation periods, and RMSE and residual standard deviations were less than 20% of the observed mean discharge, indicating satisfactory model performance. Long-term groundwater level observations from 29 monitoring wells were used to define initial hydraulic heads and to provide additional qualitative constraints on groundwater dynamics.

4. Results and Analysis

4.1. Characteristics of River and Groundwater Water Levels

The transformation relationship between river and groundwater levels was identified based on the water level elevations along each cross-section, as shown in (Figure 4). From the upstream to the downstream of the Aksu River Basin, the interactions between surface water and groundwater are as follows: At cross-section 1–1′, the relationship indicates river water recharging groundwater. At cross-section 2–2′, groundwater recharges the river. Similarly, at cross-section 3–3′, groundwater also discharges into the river. At cross-section 4–4′, the left bank shows river water recharging groundwater, whereas the right bank exhibits groundwater discharge toward the river. Based on the elevation gradient, the dominant flow direction is from groundwater to river water. At cross-section 5–5′, the left bank indicates river water recharge to groundwater, while the right bank shows groundwater discharging into the river. The overall hydraulic gradient suggests a dominant groundwater-to-river flow direction. At cross-section 6–6′, groundwater discharges into the river; at cross-section 7–7′, river water recharges groundwater; and at cross-section 8–8′, the relationship remains river-to-groundwater recharge. Based on the monitoring results of eight cross-sections between Xidaqiao and Yimanpaxia, the transformation relationship between river and groundwater exhibits pronounced spatial variability.

The upstream sections (1–2) are characterized by river water recharging groundwater, with groundwater levels clearly influenced by river stage fluctuations and shallower water tables observed near the riverbanks. The midstream sections (3–6) show groundwater discharge into the river channel, with observed groundwater levels generally higher than river stages. River water recharge is insufficient, and in certain areas, there is even a risk of river channel desiccation. In the downstream sections (7–8), the interaction pattern reverts to river water recharging groundwater. River infiltration causes a noticeable rise in groundwater levels on both sides of the riverbank. These spatial variations are closely related to basin geomorphology and aquifer structure. The upstream area consists of piedmont alluvial–proluvial fans with highly permeable riverbeds, where river water easily infiltrates to recharge groundwater. The midstream section is characterized by fine-grained alluvial plains with strong evaporation, where groundwater levels are generally higher than river stages, forming a groundwater-to-river discharge pattern. The downstream

zone transitions again into fine-grained depositional areas, where long-term river leakage intensifies, resulting in a river-to-groundwater recharge regime.

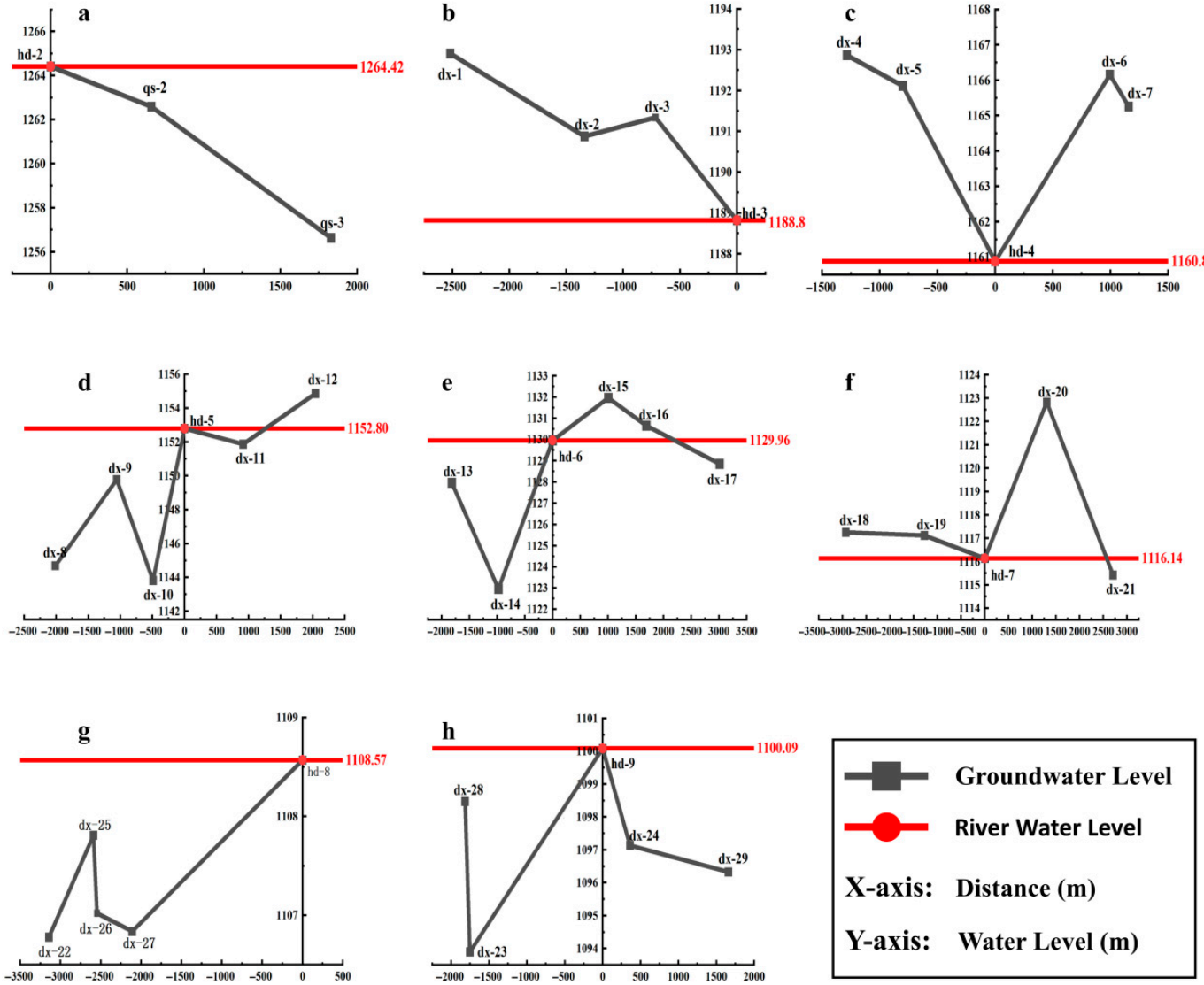

Figure 4. Lateral groundwater and river water level profiles of the eight cross-sections in the Aksu River Basin ((**a**–**h**) represent cross-sections 1–8, respectively; the spatial distribution of the river cross-sections is shown in Figure 2).

4.2. Hydrochemical Characteristics and Water Evolution Analysis

4.2.1. Spatial Distribution of Groundwater Hydrochemical Types

Based on the analysis of 305 groundwater samples, shallow groundwater in the plain area of the Aksu River Basin exhibits a pronounced longitudinal zonation in hydrochemical composition that closely corresponds to distinct stream–aquifer interaction regimes. From upstream to downstream, groundwater chemistry transitions from HCO_3^--dominated types to SO_4^{2-}- and ultimately Cl^--dominated facies, reflecting progressive shifts in recharge sources, residence time, and exchange intensity along the river corridor.

In the piedmont alluvial–proluvial fan area, groundwater is predominantly of the HCO_3^-–Ca^{2+} type, indicating rapid recharge from mountain precipitation and snowmelt infiltration with limited evaporative concentration. This hydrochemical signature is consis-

tent with losing river conditions, where river water and mountain-front recharge percolate downward to replenish the aquifer.

In the central plain, groundwater is mainly characterized by SO_4^{2-}–Ca^{2+}/Mg^{2+} types. The increased sulfate and magnesium concentrations suggest enhanced water–rock interaction and longer residence times, consistent with sustained groundwater discharge toward the river. This midstream zone therefore functions as a transitional or gaining reach, where deeper groundwater contributions modify both groundwater and river chemistry.

In the downstream fine-grained plains, groundwater is dominated by the Cl^-–Na^+ type, reflecting strong evaporative concentration and evaporite dissolution processes under arid climatic conditions. The enrichment of Na^+ and Cl^- is further amplified by irrigation return flow and groundwater abstraction, indicating intensified anthropogenic modification of natural exchange patterns. This hydrochemical regime corresponds to a downstream re-recharge zone, where river leakage and evaporative concentration jointly control groundwater salinity.

At the county scale, the observed spatial distribution of hydrochemical types mirrors this longitudinal exchange pattern, with bicarbonate-dominated groundwater prevalent in upstream recharge areas and chloride-dominated groundwater concentrated in downstream discharge and evaporation-dominated zones. Overall, the spatial succession of groundwater facies provides process-based evidence for a three-stage stream–aquifer interaction framework: upstream recharge, midstream discharge, and downstream re-recharge under strong evaporative and anthropogenic influences.

4.2.2. Comparison of River and Groundwater Chemical Compositions

According to (Table 1) and (Table S1, see Supplementary Materials for details) both river water and groundwater in the Aksu River Basin are generally weakly alkaline, with pH values ranging from 7.08 to 7.71 and very low variability, indicating relatively stable acid–base conditions across the basin. However, substantial differences in solute concentrations between river water and groundwater reveal distinct geochemical evolution pathways and exchange dynamics.

Table 1. Major hydrochemical characteristics of river water and groundwater in the Aksu River Basin.

Type	Parameter	pH	K^+	Na^+	Ca^{2+}	Mg^{2+}	Cl^-	SO_4^{2-}	HCO_3^-	TDS
River water	Maximum	7.71	24.86	141.32	309.32	196.30	224.30	1022.76	720.31	2.28
	Minimum	7.13	2.76	4.41	37.18	11.80	4.78	73.19	140.02	0.22
	Mean	7.54	12.92	22.74	66.96	40.21	32.88	168.26	221.10	0.45
	Coefficient of variation	0.02	0.40	1.74	1.20	1.30	1.94	1.68	0.76	1.33
Groundwater	Maximum	7.61	59.89	1066.60	449.06	477.54	977.49	3559.53	510.90	6.80
	Minimum	7.08	2.28	5.90	33.82	16.40	4.62	88.69	102.18	0.26
	Mean	7.34	12.48	149.52	124.64	85.41	180.91	496.29	296.06	1.20
	Coefficient of variation	0.02	0.90	9.24	1.31	2.25	6.24	3.98	0.50	2.78

The total dissolved solids (TDS) range from 0.22 to 6.80 g/L. The mean TDS of river water is 0.45 g/L, whereas that of groundwater reaches 1.20 g/L (Table 1), indicating significantly higher mineralization in the aquifer system. This contrast suggests that groundwater undergoes longer subsurface flow paths and more intensive water–rock interaction compared to river water, which is continuously renewed by upstream inflow.

In terms of major ions (Table 1), river water is characterized by HCO_3^- (221 mg/L) > SO_4^{2-} (168 mg/L) > Cl^- (33 mg/L) for anions and Ca^{2+} (67 mg/L) > Mg^{2+} (40 mg/L)

> Na^+ (23 mg/L) > K^+ (13 mg/L) for cations, clearly reflecting a Ca–HCO_3 end-member controlled primarily by carbonate weathering in the mountainous recharge area. In contrast, groundwater shows SO_4^{2-} (496 mg/L) > HCO_3^- (296 mg/L) > Cl^- (181 mg/L) for anions and Na^+ (150 mg/L) > Ca^{2+} (125 mg/L) > Mg^{2+} (85 mg/L) > K^+ (12 mg/L) for cations, exhibiting a pronounced evaporite and ion-exchange signature. The enrichment of Na^+, Cl^-, and SO_4^{2-} in groundwater reflects cumulative effects of mineral dissolution, evaporative concentration, and agricultural return flow during subsurface transport.

Variability analysis further highlights the contrasting hydrochemical stability of river water and groundwater (Table 1). The coefficients of variation (CVs) for Na^+, Cl^-, SO_4^{2-}, and TDS in groundwater (9.24, 6.24, 3.98, and 2.78, respectively) are substantially higher than those in river water (1.74, 1.94, 1.68, and 1.33). This pronounced heterogeneity indicates spatially variable recharge–discharge conditions and localized geochemical modification within the aquifer system, consistent with zones of intensified groundwater discharge and anthropogenic disturbance.

Sectional statistics (Table S1) provide further insight into stream–aquifer exchange intensity. Midstream cross-section 6 represents a pronounced zone of chemical enrichment, where Na^+ reaches 1066.6 mg/L, SO_4^{2-} reaches 3559.5 mg/L, and TDS reaches 6.80 g/L—values significantly higher than those at other sections. Such extreme enrichment suggests concentrated groundwater discharge combined with evaporite dissolution and evaporative concentration, identifying this reach as a hotspot of river–groundwater interaction. The superposition of elevated salinity and spatial variability at this section supports the interpretation of an active exchange interface between the river and the aquifer.

Overall, the systematic differences between river water and groundwater chemistry documented in Tables 1 and S1 provide process-based evidence for identifying recharge–discharge relationships. River water maintains relatively stable carbonate-dominated composition, whereas groundwater chemistry reflects cumulative geochemical evolution and anthropogenic modification, thereby serving as a sensitive tracer of stream–aquifer interaction intensity across the basin.

4.2.3. Ionic Variation Characteristics

According to (Figure 5) and (Table S2, see Supplementary Materials for details), the hydrochemical composition of river water and groundwater in the Aksu River Basin exhibits pronounced differences among the cross-sections. At cross-section 1, Ca^{2+} and Mg^{2+} account for the highest proportions (66.10% and 42.42%), forming a typical Ca–Mg–HCO_3-type water dominated by carbonate dissolution. At cross-section 2, the proportion of Na^+ + K^+ increases to 14–19%, indicating the influence of evaporite dissolution or groundwater mixing. From cross-sections 3 to 8, Ca^{2+} and Mg^{2+} are the dominant cations, while SO_4^{2-} and HCO_3^- are the major anions, though spatial variations are pronounced. At cross-section 5, Mg^{2+} shows the highest proportion (47.24%), whereas at section 7, it is the lowest (13.28%). At section 6, SO_4^{2-} reaches 68.24%, while HCO_3^- peaks at 64.26%, indicating the coexistence of evaporative concentration and river–groundwater mixing processes. In the downstream cross-section 8, Na^+ + K^+ exhibit the highest proportion (67.52%), while Ca^{2+} shows the lowest (16.93%), suggesting a transition in water type from carbonate-dominated to sulfate–sodium-dominated. Overall, the proportions of Na^+ + K^+ and Cl^- increase downstream, whereas Ca^{2+} and HCO_3^- gradually decrease, revealing a hydrochemical evolution from upstream carbonate weathering to downstream evaporite and saline mineral dissolution control. Gibbs diagrams (Figure 6) further demonstrate that river-water samples mainly fall within the rock-weathering control field or transition toward the evaporation–crystallization field. In contrast, groundwater samples are more widely scattered, with some extending into the evaporation–crystallization domain, and ex-

hibit markedly higher TDS values than river water (locally > 6000 mg/L). This indicates that groundwater, in addition to being influenced by weathering processes, is strongly affected by evaporative concentration and saline mineral dissolution. The ratio $Cl^- / (Cl^- + HCO_3^-)$ is generally high, reflecting the combined effects of agricultural return flow and evaporite dissolution. In summary, the hydrochemical evolution in the Aksu River Basin follows a general pattern of "upstream rock weathering → midstream mixing transition → downstream evaporation–crystallization control." River water remains relatively stable, predominantly of the Ca–HCO_3 type, whereas groundwater exhibits greater compositional variability and is more strongly influenced by evaporation, leaching, and anthropogenic activities. In particular, the midstream sections (e.g., section 6) represent the most active zones of hydrochemical transformation and river–groundwater exchange. Downstream waters progressively evolve into evaporation-dominated types enriched in Na^+, SO_4^{2-}, and Cl^-, providing key evidence for identifying river–groundwater recharge–discharge relationships.

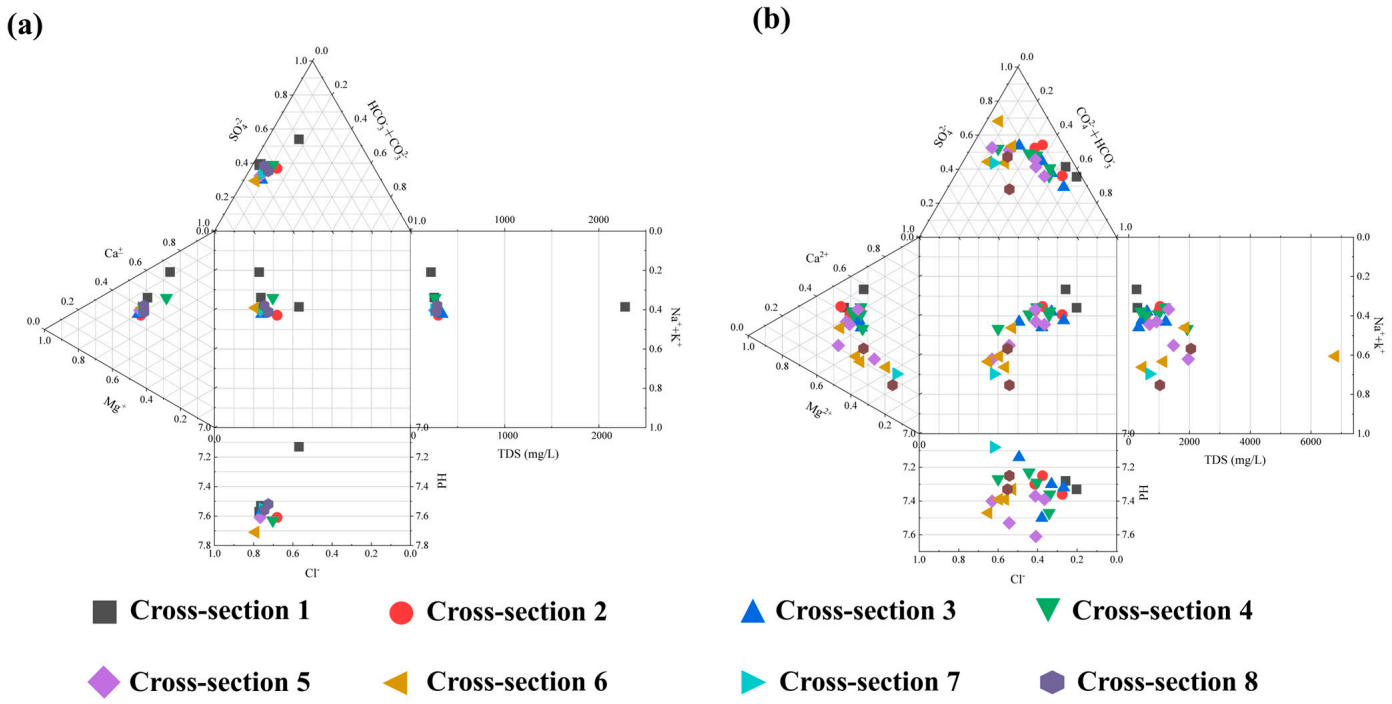

Figure 5. Piper diagram of the ionic composition of river water (**a**) and groundwater (**b**) in the Aksu River Basin.

4.3. Stable Isotope Signatures and Recharge Relationships

4.3.1. Mineralization Indicator

To characterize the hydraulic relationship between river water and groundwater in the Aksu River Basin, this study employs total dissolved solids (TDS), electrical conductivity (EC), the Cl^- / SO_4^{2-} ratio, and Gibbs diagrams as complementary hydrochemical indicators. These indicators are used to identify spatial patterns of mineralization, mixing, and exchange intensity rather than serving as standalone quantitative proof of recharge–discharge mechanisms. Instead, they provide essential geochemical context for interpreting stream–aquifer interactions in conjunction with isotopic and hydraulic evidence.

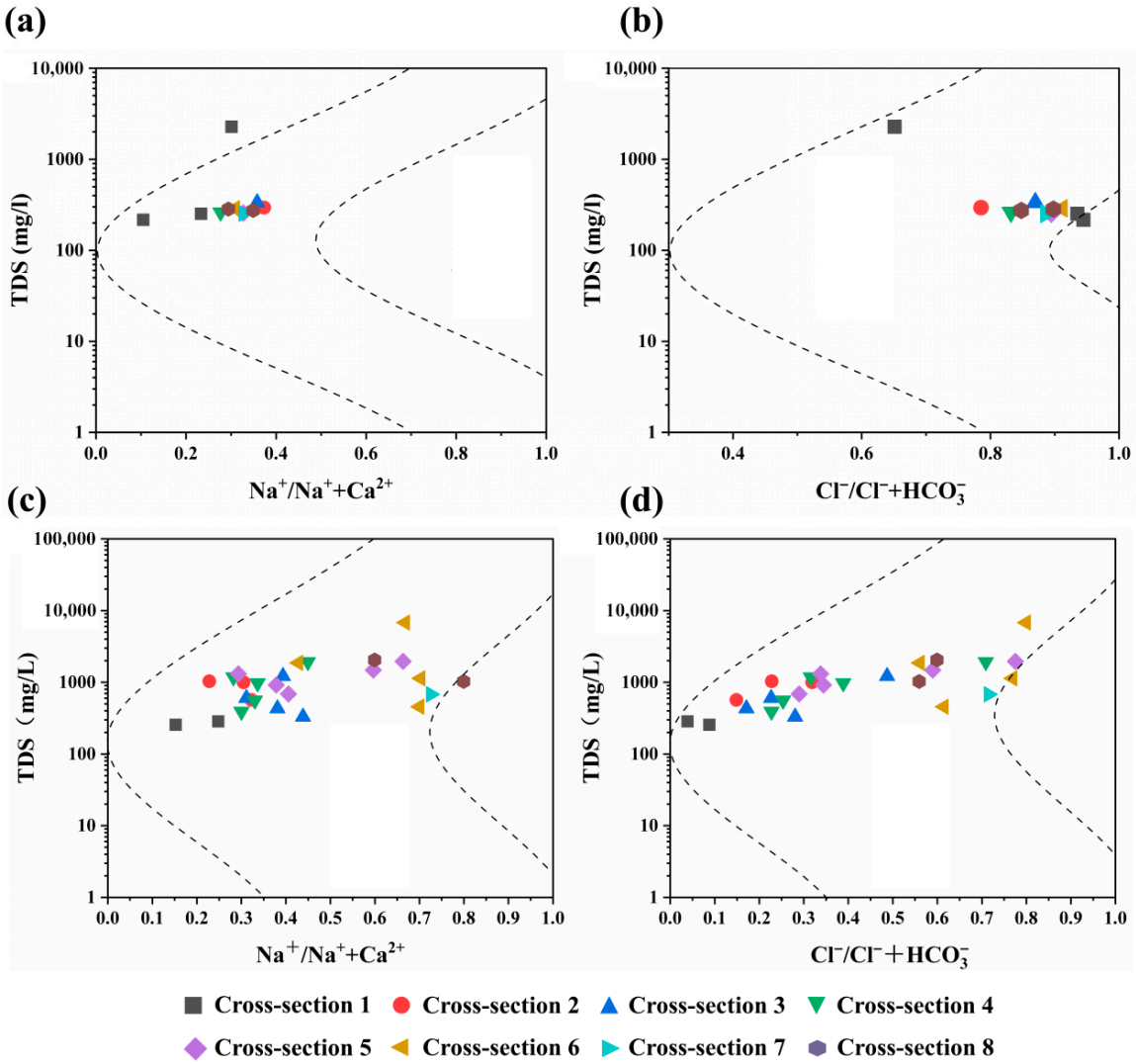

Figure 6. Gibbs diagrams of river water and groundwater in the Aksu River Basin: (**a**,**b**) represent river water; (**c**,**d**) represent groundwater.

As shown in Figure 7, groundwater exhibits substantially higher TDS and EC values than river water, reflecting longer residence times and stronger water–rock interaction within the aquifer system. Both TDS and EC reach peak values at cross-section 6, indicating pronounced mineral enrichment in the midstream reach. Along the longitudinal profile, river water TDS and EC show relatively limited variation, whereas groundwater exhibits a clear pattern of decrease in upstream sections (1–3), sharp increase in midstream sections (3–6), and gradual decline downstream (6–8). This contrasting behavior reflects spatially variable exchange regimes between river water and groundwater.

The inverse variation pattern between river water and groundwater, together with the ion cross-sectional profiles (Figures 8 and 9) and Gibbs diagrams (Figure 6), indicates a spatially organized exchange system characterized by upstream river infiltration, midstream groundwater discharge to the river, and downstream renewed river infiltration. In particular, the strong mineral enrichment observed at cross-section 6 suggests sustained groundwater discharge combined with evaporite dissolution, identifying this reach as an active zone of stream–aquifer interaction.

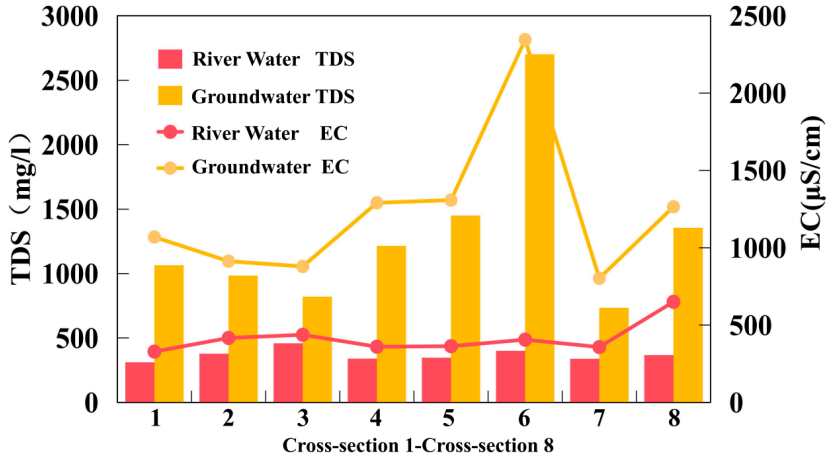

Figure 7. Variations of EC and TDS for river water and groundwater along the cross-sections in the Aksu River Basin.

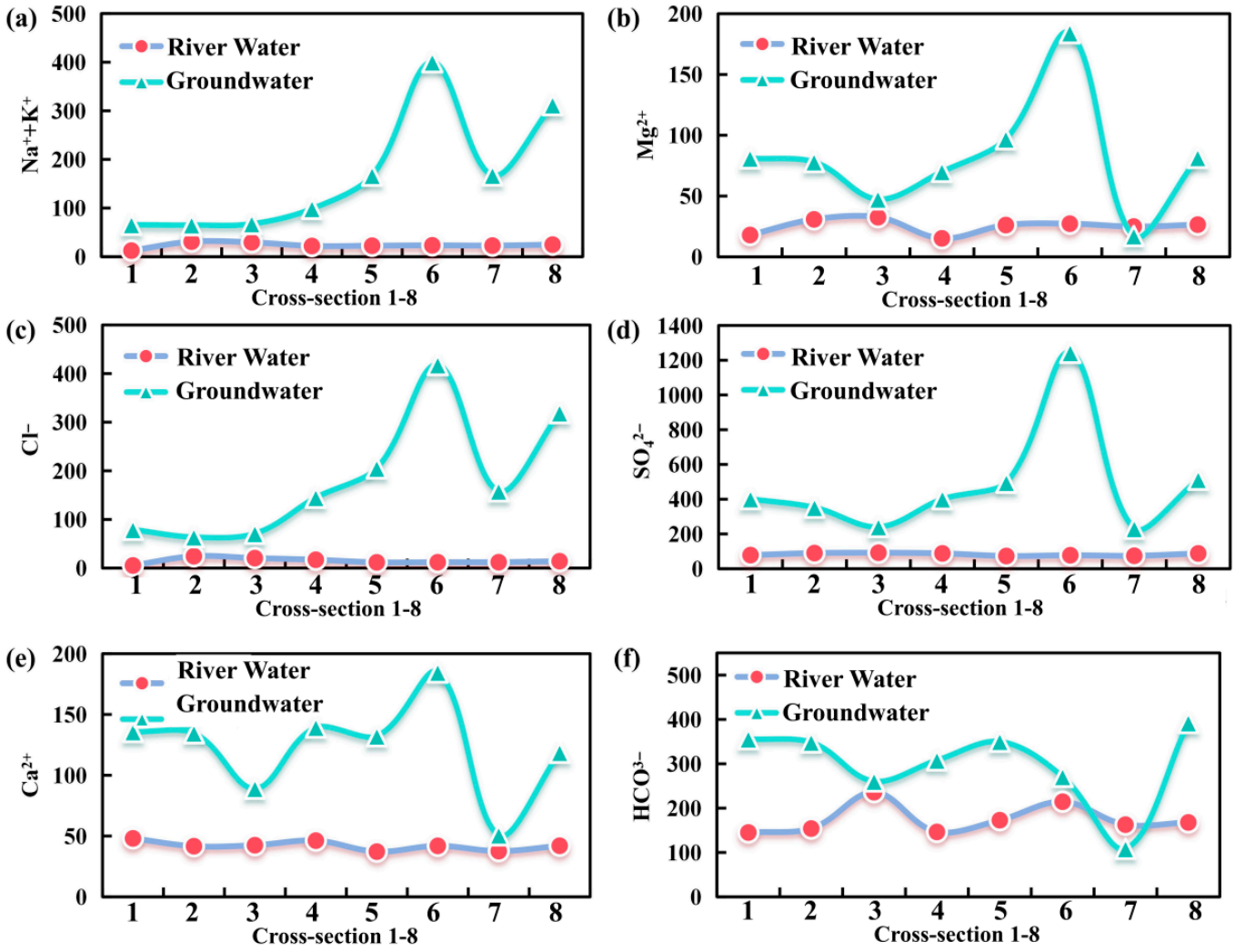

Figure 8. Longitudinal variations of ionic concentrations in river water and groundwater along the Aksu River Basin cross-sections. (**a**) $Na^+ + K^+$; (**b**) Mg^{2+}; (**c**) Cl^-; (**d**) $SO_4{}^{2-}$; (**e**) Ca^{2+}; and (**f**) $HCO_3{}^-$.

https://doi.org/10.3390/hydrology13030095

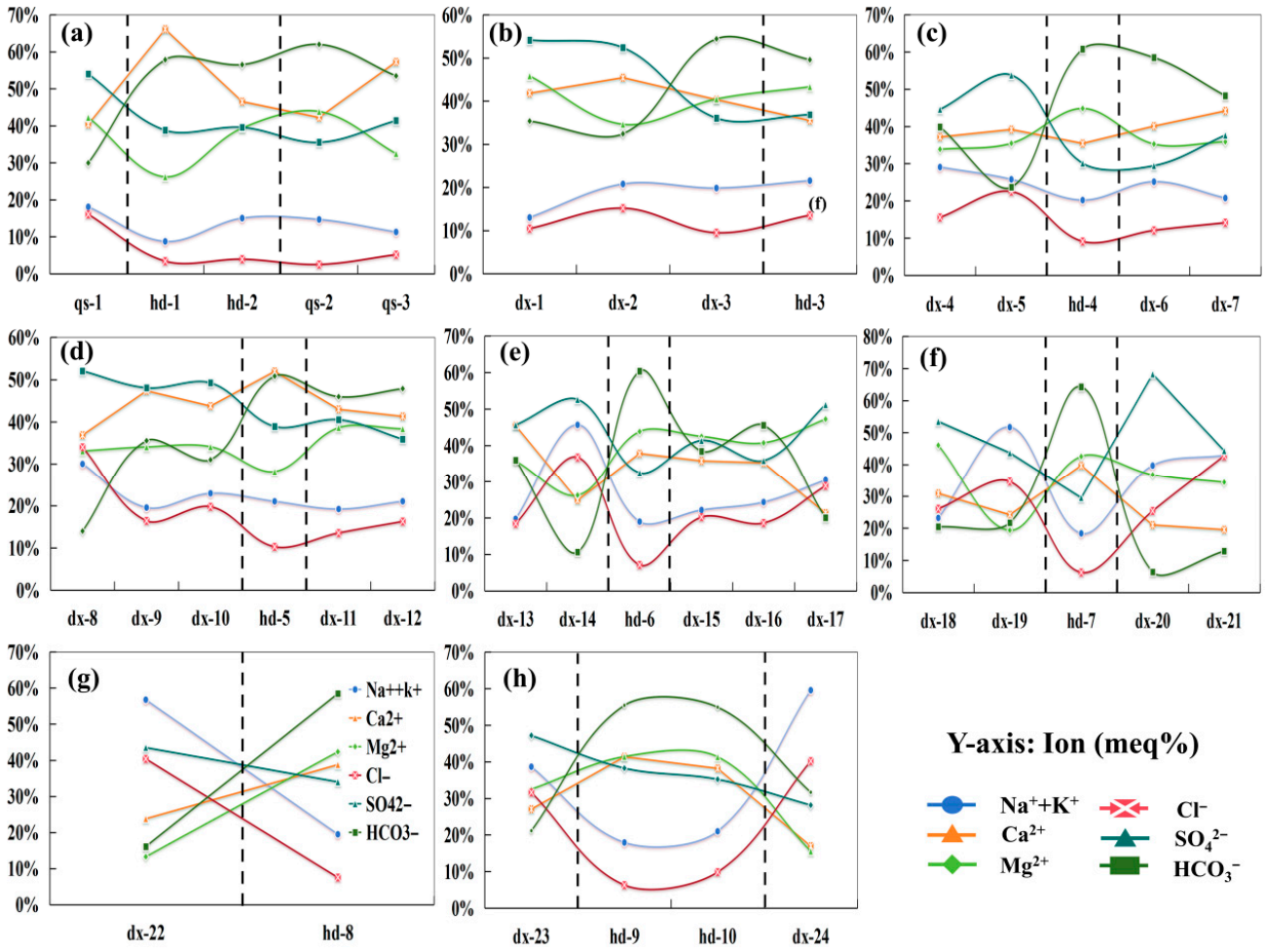

Figure 9. Lateral variations of major ions in river water and groundwater across the eight cross-sections (dashed areas indicate river channels; areas outside the dashed lines represent the left and right riverbanks; (**a**–**h**) correspond to cross-sections 1–8, respectively).

Because TDS and EC are sensitive to evaporative concentration and irrigation return flow, they are used primarily as indicators of overall mineralization trends rather than definitive tracers of hydraulic exchange direction. Therefore, conservative ions such as Cl^- and Na^+, along with the Na^+/Cl^- ratio and hydraulic gradients, provide more reliable constraints on recharge–discharge relationships. The high consistency among these independent indicators strengthens the interpretation of spatially variable stream–aquifer exchange intensity across the basin.

4.3.2. Ion Concentration Indicator

Figure 8 illustrates pronounced longitudinal differences in major ion concentrations between river water and groundwater in the Aksu River Basin, reflecting distinct geochemical evolution pathways and exchange dynamics. Overall, groundwater exhibits significantly higher concentrations of most major ions than river water, indicating cumulative effects of mineral dissolution, evaporative concentration, and longer subsurface flow paths. In contrast, river water maintains relatively stable ion concentrations due to continuous replenishment from upstream recharge.

While longitudinal variations in TDS provide useful first-order information on mineralization trends, they do not distinguish which specific solutes control exchange processes or resolve superimposed geochemical effects. Therefore, examination of individual ion behavior provides more robust mechanistic insight into stream–aquifer interactions.

At cross-sections 3 and 7, multiple ions—including Na^++K^+, Cl^-, Ca^{2+}, SO_4^{2-}, Mg^{2+}, and HCO_3^-—exhibit clear convergence or interlacing trends between river water and groundwater (Figure 8). At cross-section 3, river water ion concentrations increase while groundwater concentrations decrease and converge, indicating weakening groundwater discharge and a transition toward river-to-groundwater recharge conditions. At cross-section 7, conservative ions such as Na^++K^+ and Cl^- in groundwater approach river water concentrations, and Mg^{2+} and HCO_3^- even decrease below river water values, indicating intensified river infiltration into the aquifer in the downstream reach.

It is important to note that HCO_3^-, Ca^{2+}, and Mg^{2+} are influenced not only by hydraulic exchange but also by carbonate dissolution, evaporite interaction, and ion-exchange processes. Therefore, variations in these ions reflect both geochemical reactions and hydrological exchange. In contrast, conservative ions such as Cl^- and Na^+ are minimally affected by mineral precipitation or adsorption and thus serve as more reliable tracers of recharge–discharge relationships. The convergence of conservative ion concentrations between river water and groundwater at cross-sections 3 and 7 therefore provides strong geochemical evidence for exchange reversal zones, where the direction of stream–aquifer interaction shifts spatially.

Figure 9 further illustrates the lateral distribution of ionic compositions across river cross-sections. River water is consistently dominated by HCO_3^- and Ca^{2+}, reflecting a Ca–HCO_3 hydrochemical signature characteristic of mountain recharge sources. In contrast, adjacent groundwater is generally enriched in Cl^-, SO_4^{2-}, and Na^+, reflecting evaporite dissolution, evaporative concentration, and anthropogenic return flow.

At cross-section 1, the ionic composition of right-bank spring samples (qs-2 and qs-3) closely matches that of river water, indicating direct river recharge to shallow groundwater. At cross-section 2, increasing Na^+ fractions in groundwater near the river further support river infiltration. In contrast, at cross-sections 3–5, elevated Na^+ and Mg^{2+} concentrations in groundwater relative to river water indicate groundwater discharge into the river. At cross-sections 6–8, progressive decreases in Na^+ and SO_4^{2-} and increases in HCO_3^- in near-bank groundwater indicate renewed river infiltration and dilution effects.

Overall, the spatial convergence and divergence patterns of conservative ions shown in Figures 8 and 9 provide process-based geochemical evidence for a longitudinal exchange framework characterized by upstream river infiltration, midstream groundwater discharge, and downstream renewed river recharge. These hydrochemical indicators establish a critical geochemical foundation for interpreting recharge–discharge relationships, which are further evaluated using stable isotope signatures in the following sections.

4.3.3. Stable Isotope Characteristics and Recharge Relationship Analysis

Local Meteoric Water Line (LMWL) The water cycle in arid northwestern China is complex, and hydrogen–oxygen stable isotopes effectively reflect the sources and evolution of atmospheric moisture. Due to the lack of long-term precipitation isotope observations in the Aksu River Basin, this study used data from the Global Network of Isotopes in Precipitation (GNIP, http://www.iaea.org, accessed on 10 March 2025) and compared them with the Global Meteoric Water Line (GMWL: $\delta D = 8\delta^{18}O + 10$) [70]. The results (Figure 10a) show that the slope of the meteoric water line at the Aksu Batuan Station is 7.66, slightly lower than that of the GMWL (8.0), which is consistent with the strong evaporative characteristics typical of arid regions. Seasonally, precipitation is isotopically enriched in summer and depleted in winter, and the isotope variations correspond to the precipitation trend with a certain lag effect. The deuterium-excess (d-excess) parameter further indicates that due to intense re-evaporation, both δD and $\delta^{18}O$ values in the study area are relatively elevated [71].

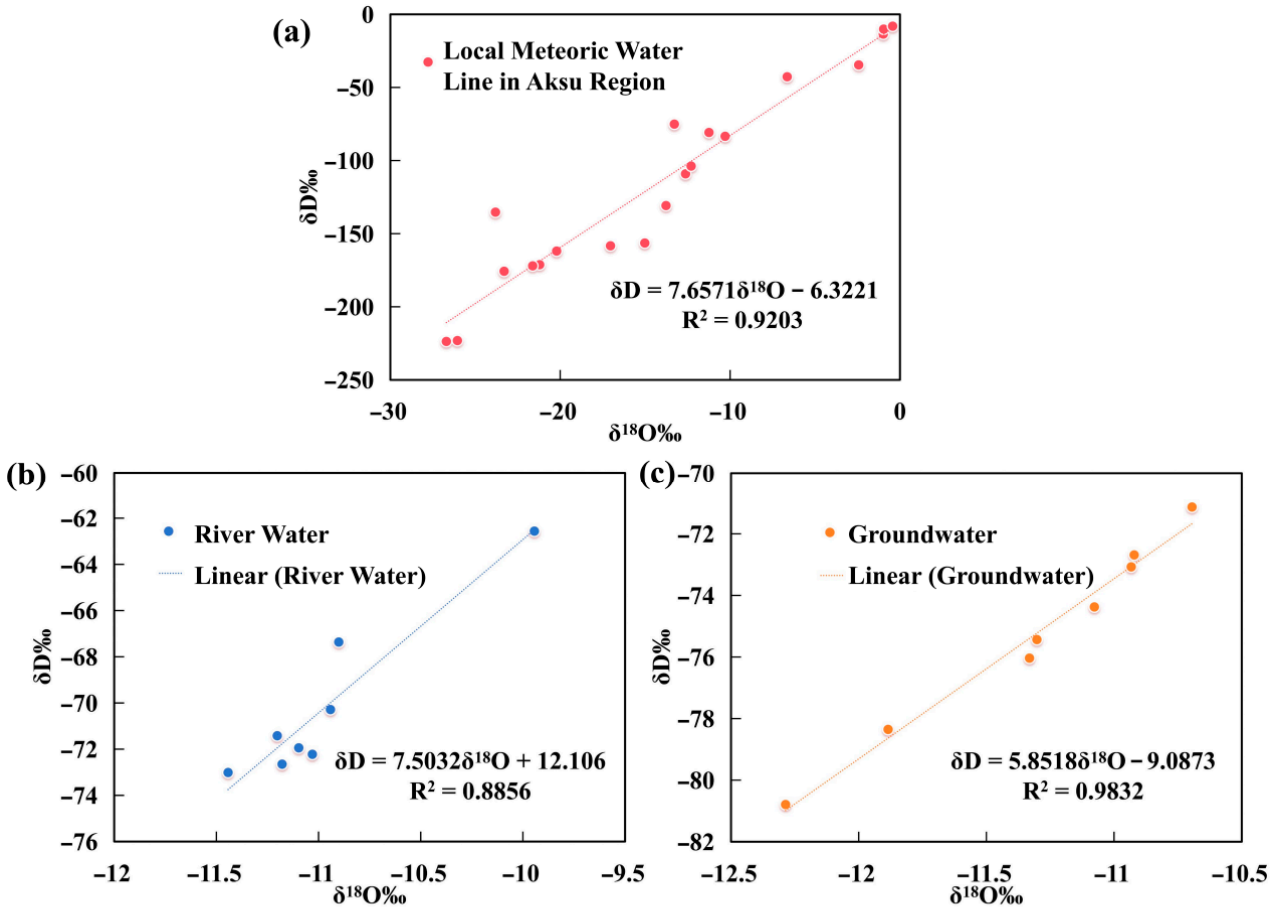

Figure 10. (**a**) Slope of the local meteoric water line in the study area; (**b**) δD–δ^{18}O relationship in river water; (**c**) δD–δ^{18}O relationship in groundwater along the Aksu River cross-sections.

4.3.4. Longitudinal Variations of δD and δ^{18}O in River and Groundwater

The isotope analysis of river water and groundwater (Figure 10a,b) provides critical constraints on recharge sources and stream–aquifer exchange processes in the Aksu River Basin. Across the basin, δD values range from –62.56‰ to –81.71‰, and δ^{18}O values range from –9.94‰ to –12.49‰, indicating that both river water and groundwater originate primarily from meteoric precipitation and mountain recharge sources.

River water exhibits relatively enriched isotopic compositions, with δD values ranging from –62.56‰ to –73.41‰ and δ^{18}O values ranging from –9.94‰ to –11.48‰, approximately 6–9‰ (δD) and 0.3–1‰ (δ^{18}O) higher than those of groundwater. In contrast, groundwater shows more depleted isotopic signatures, reflecting longer subsurface residence times and recharge dominated by precipitation and snowmelt infiltration. This isotopic distinction provides clear evidence of differing recharge histories and hydrological pathways between surface water and groundwater.

Both river water and groundwater samples exhibit strong linear relationships, with regression equations of $\delta D = 7.503\delta^{18}O + 12.106$ and $\delta D = 5.852\delta^{18}O - 9.087$, respectively (Figure 10). The slopes of both regression lines are lower than that of the regional meteoric water line ($\delta D = 7.657\delta^{18}O - 6.322$), indicating that evaporation exerts a significant influence on isotopic composition during surface flow and shallow groundwater circulation. The stronger deviation of groundwater from the meteoric water line reflects cumulative evaporative enrichment and geochemical modification during subsurface transport.

Longitudinal variations in mean isotope values (Figure 11) further reveal spatially variable stream–aquifer exchange intensity. Groundwater samples located near the river

channel exhibit relatively enriched isotopic compositions, closely approaching river water signatures, indicating direct hydraulic connectivity and active river recharge to the aquifer. In contrast, groundwater samples located farther from the river show more depleted isotopic compositions, reflecting recharge from precipitation and longer residence times with limited river influence.

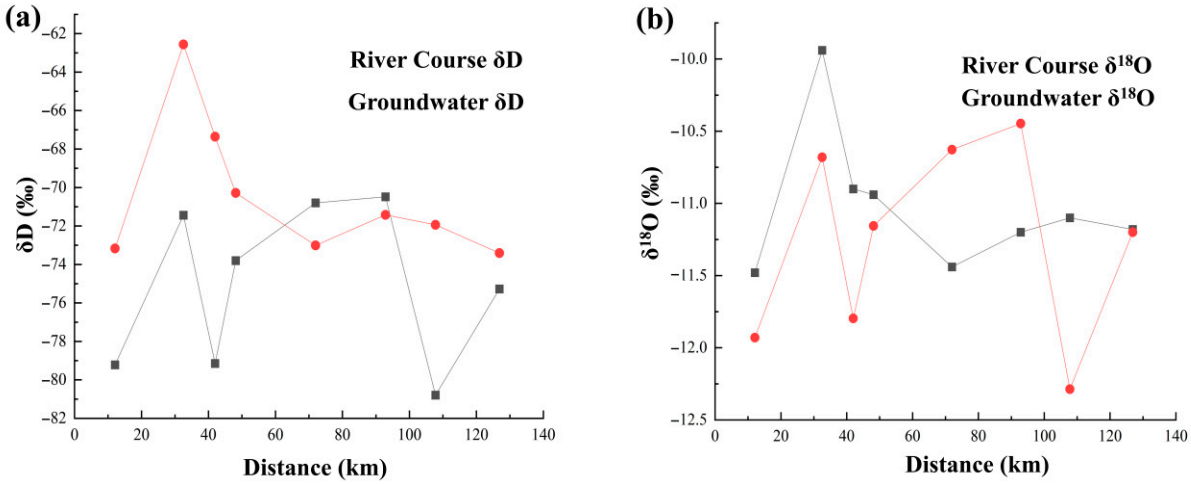

Figure 11. Longitudinal variations of mean δD (**a**) and $\delta^{18}O$ (**b**) values in river water and groundwater along the Aksu River Basin.

This spatial isotopic gradient provides direct tracer evidence of recharge–discharge relationships along the river corridor. The progressive isotopic convergence between river water and groundwater in downstream reaches confirms intensified river infiltration, whereas the isotopic depletion of groundwater relative to river water in midstream sections reflects dominant groundwater discharge to the river. These isotope-based interpretations are consistent with hydrochemical indicators such as Cl^-, Na^+, and TDS variations (Figures 7–9), demonstrating strong agreement between independent tracers of stream–aquifer interaction.

4.3.5. Runoff Recharge Proportion Analysis Based on the MixSIAR Model

To quantitatively evaluate recharge–discharge relationships, the MixSIAR isotope mixing model was applied to estimate source contribution rates of river water and groundwater along different cross-sections in the Aksu River Basin (Table 2). This model provides quantitative constraints on stream–aquifer exchange processes by resolving the relative contributions of river water infiltration and groundwater discharge.

The results show clear spatial variation in source contributions along the river course. At upstream cross-section 1 and downstream cross-sections 7 and 8, river water contributions dominate (Table 2), indicating that groundwater in these areas is primarily recharged by river infiltration. This pattern is consistent with the enriched isotopic signatures of groundwater observed near the river channel (Figure 11) and supports the interpretation of losing-stream conditions in these reaches.

In contrast, groundwater contributions exceed 0.77 at cross-sections 2–6, indicating that these river reaches are primarily sustained by groundwater discharge and function as gaining-stream segments. Particularly at cross-sections 4 and 5, groundwater contribution rates reach 0.89–0.91 with narrow credible intervals, demonstrating high confidence in the estimated baseflow contribution. These findings are consistent with hydrochemical evidence of elevated Na^+, Cl^-, and TDS concentrations in groundwater (Tables 1 and S1), reflecting prolonged subsurface flow and discharge to the river.

Table 2. Contribution rates of river water, precipitation, and spring water to groundwater along the Aksu River cross-sections.

Type		Contribution Rate	Standard Deviation	Confidence Interval						
Cross-section 1	River water	0.542	0.229	0.074	0.129	0.38	0.565	0.72	0.884	0.907
	Precipitation	0.072	0.023	0.036	0.041	0.056	0.068	0.083	0.115	0.128
	Spring water	0.387	0.225	0.026	0.044	0.213	0.364	0.548	0.791	0.84
Cross-section 2	River water	0.063	0.046	0.003	0.006	0.028	0.055	0.088	0.143	0.172
	Precipitation	0.057	0.035	0.003	0.006	0.03	0.053	0.077	0.12	0.137
	groundwater	0.881	0.049	0.761	0.793	0.858	0.889	0.914	0.943	0.951
Cross-section 3	River water	0.331	0.136	0.058	0.095	0.247	0.332	0.415	0.558	0.607
	Precipitation	0.191	0.134	0.01	0.02	0.085	0.165	0.275	0.44	0.492
	groundwater	0.478	0.127	0.171	0.243	0.406	0.495	0.57	0.652	0.678
Cross-section 4	River water	0.052	0.038	0.002	0.005	0.024	0.046	0.073	0.123	0.142
	Precipitation	0.057	0.031	0.005	0.009	0.036	0.056	0.076	0.113	0.126
	groundwater	0.89	0.04	0.79	0.816	0.871	0.899	0.917	0.941	0.948
Cross-section 5	River water	0.046	0.034	0.002	0.004	0.021	0.04	0.064	0.112	0.128
	Precipitation	0.048	0.03	0.003	0.005	0.025	0.045	0.066	0.101	0.116
	groundwater	0.906	0.041	0.803	0.833	0.885	0.912	0.934	0.959	0.968
Cross-section 6	River water	0.115	0.108	0.004	0.007	0.038	0.084	0.159	0.332	0.408
	Precipitation	0.106	0.09	0.004	0.009	0.041	0.08	0.145	0.289	0.35
	groundwater	0.779	0.155	0.373	0.466	0.708	0.821	0.89	0.952	0.968
Cross-section 7	River water	0.389	0.192	0.041	0.076	0.248	0.388	0.523	0.715	0.764
	Precipitation	0.293	0.165	0.033	0.051	0.168	0.276	0.401	0.598	0.65
	groundwater	0.318	0.178	0.037	0.056	0.182	0.3	0.435	0.634	0.701
Cross-section 8	River water	0.471	0.269	0.029	0.051	0.22	0.459	0.693	0.882	0.906
	Precipitation	0.074	0.023	0.041	0.045	0.058	0.07	0.085	0.115	0.128
	groundwater	0.456	0.271	0.022	0.045	0.234	0.467	0.708	0.881	0.903

At cross-section 7, the contributions of multiple end-members are relatively similar and associated with larger uncertainty ranges, indicating an important transition zone where recharge–discharge relationships shift. This transitional behavior is also reflected in hydrochemical convergence patterns and isotopic enrichment gradients (Figures 8–11), demonstrating the combined influence of river infiltration and groundwater discharge.

Overall, MixSIAR results quantitatively confirm a longitudinal exchange framework characterized by upstream river infiltration, midstream groundwater discharge, and downstream renewed river infiltration. This pattern is fully consistent with independent hydrochemical indicators, TDS/EC trends, and Gibbs diagram interpretations (Figures 6–11), providing integrated multi-tracer evidence for spatial differentiation in stream–aquifer interaction processes across the basin.

4.4. MIKE SHE Simulation Results and Model Validation

4.4.1. Model Identification and Validation

To quantitatively characterize the river–groundwater interaction processes in the Aksu River Basin, this study applied the MIKE SHE distributed hydrological model. The model integrates five core modules—evapotranspiration (ET), overland flow (OL), channel flow (OC), unsaturated zone flow (UZ), and saturated zone flow (SZ)—which together represent the complete hydrological cycle of the basin. Model calibration combined automatic

optimization and manual adjustment. Key parameters—including Manning's roughness coefficient, riverbed hydraulic conductivity, saturated hydraulic conductivity, specific yield, and storage coefficient—were iteratively tuned to ensure both physical realism and regional applicability (Table 3). The period 2010–2017 was selected for calibration and 2018–2021 for validation. Daily discharge at two hydrological control stations—Xidaqiao and Yimanpaxia—was simulated and compared with observations. Model performance was evaluated using the root mean square error (RMSE), standard deviation of residuals (STDres), and coefficient of determination (R^2). Results showed that both RMSE and STDres were less than 20% of the observed mean discharge during the calibration and validation periods, with R^2 values exceeding 0.7 (Table 4), confirming the reliability of the parameter calibration. During the calibration period, the correlation between observed and simulated discharge at Xidaqiao reached 0.86, increasing to 0.91 during validation. At Yimanpaxia, the corresponding values were 0.84 and 0.90, indicating good overall agreement. The model successfully reproduced the seasonal discharge pattern of the Aksu River, with peak flows in June–August and low flows from October to March, reflecting the combined influence of snowmelt and anthropogenic water use. The simulated discharge at Xidaqiao was slightly higher than the observed value (R^2 = 0.89), while that at Yimanpaxia was slightly lower (R^2 = 0.79), showing a consistent overall trend (Figure 12). The scatter plots for the calibration and validation periods (Figure 13a–d) indicate that the model achieved higher accuracy at low flows, with minor deviations during high-flow periods.Overall, the model effectively captured both the seasonal transitions and spatial variability of discharge, demonstrating strong dynamic reproducibility and providing quantitative support for the identified pattern of "upstream river recharge–midstream groundwater discharge–downstream river infiltration."

Table 3. Calibrated parameters and values of the MIKE SHE model.

Module	Calibrated Parameter	Unit	Calibrated Value
Overland flow	Manning's coefficient	$m^{1/3}\cdot s^{-1}$	0.02
River channel	Channel roughness coefficient	$m^{1/3}\cdot s^{-1}$	33.33
	Riverbed hydraulic conductivity	$m\cdot s^{-1}$	6.5×10^{-7}
Unsaturated zone	Saturated soil hydraulic conductivity	$m\cdot s^{-1}$	1×10^{-5}~1×10^{-5}
Saturated zone	Specific yield	--	0.125
	Horizontal hydraulic conductivity	$m\cdot s^{-1}$	4×10^{-4}~9×10^{-5}
	Vertical hydraulic conductivity	$m\cdot s^{-1}$	4×10^{-5}~9×10^{-5}
	Storage coefficient	--	1×10^{-4}

Table 4. Evaluation results of simulated and observed streamflow at the hydrological stations.

Evaluation Index	Xidaqiao Station		Yimanpaxia Gate	
	Calibration Period	Validation Period	Calibration Period	Validation Period
RMSE	80.82	32.46	82.89	48.03
STDres	81.34	29.72	82.33	48.36
R^2	0.86	0.91	0.84	0.90

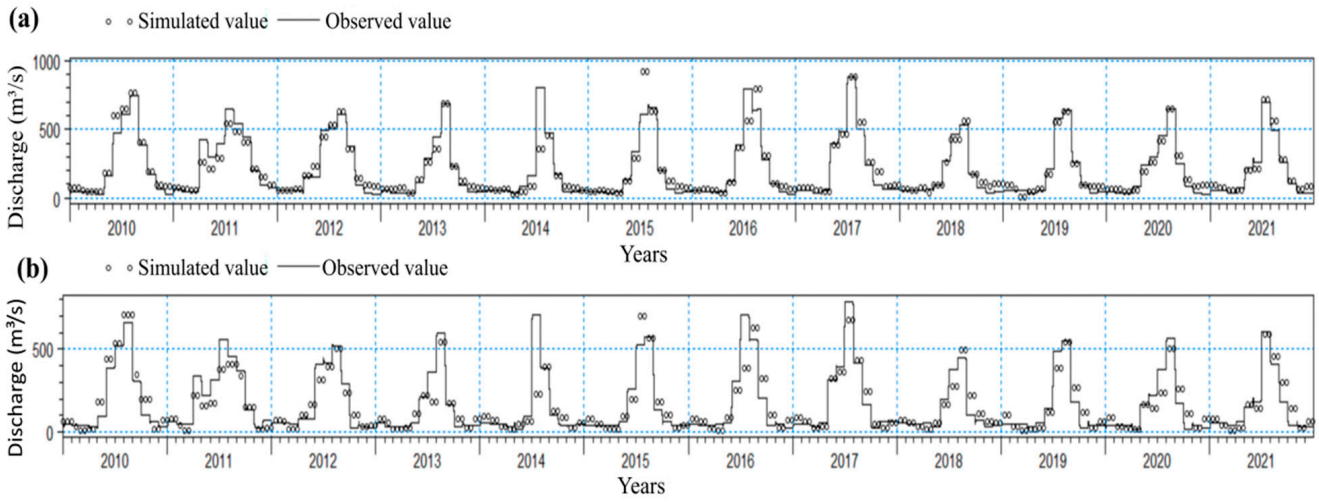

Figure 12. Comparison between simulated and observed streamflow at Xidaqiao (**a**) and Yimanpaxia Gate (**b**) hydrological stations.

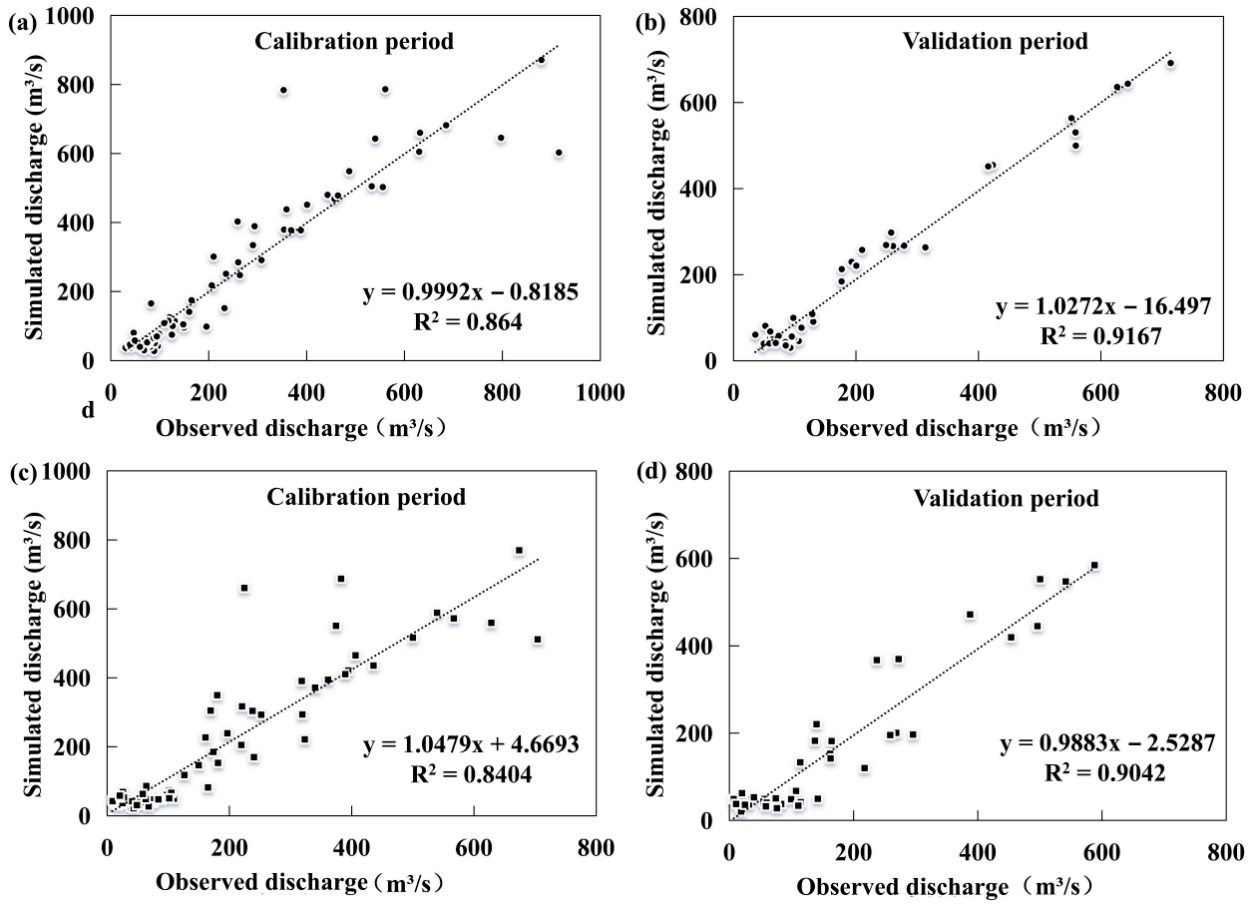

Figure 13. Correlation between simulated and observed discharge during calibration and validation periods: (**a**,**b**) Xidaqiao Station; (**c**,**d**) Yimanpaxia Gate.

4.4.2. Model Uncertainty

Although the MIKE SHE model comprehensively represents hydrological processes, its accuracy remains influenced by data quality, structural assumptions, and parameter simplifications. The model employed Darcy's law to describe saturated flow and simplified the vegetation interception and bidirectional surface–groundwater coupling processes, which may introduce uncertainties during extreme events. Due to limited regional observations,

calibration and validation relied only on the Xidaqiao and Yimanpaxia stations, which may reduce parameter representativeness. Moreover, the model's computational demand and potential overfitting during calibration suggest the need for additional groundwater monitoring wells and field data to improve simulation accuracy for spatial heterogeneity. Overall, the model validation results are highly consistent with evidence from water levels, hydrochemistry, and stable isotopes regarding recharge–discharge direction, spatial pattern, and seasonal dynamics, further strengthening the integrated understanding of river–groundwater interactions in the Aksu River plain.

The MIKE SHE model simulations revealed significant spatio-temporal feedbacks between river water and groundwater in the Aksu River Basin. The model achieved high accuracy ($R^2 > 0.84$) during both calibration and validation, effectively reproducing the bidirectional recharge–discharge processes associated with seasonal flow transitions. Combined with water-level, hydrochemical, and isotopic analyses, the results confirm a typical pattern of "upstream river recharge–midstream groundwater discharge–downstream river recharge." The modeling outcomes not only verified the consistency among multiple lines of evidence but also provided scientific support for understanding river–groundwater coupling mechanisms and formulating groundwater abstraction control, water-saving, and integrated management policies in arid regions.

5. Discussion

Based on four complementary lines of evidence—water level observations, hydrochemistry, isotope analysis, and numerical modeling—this study elucidates the mechanisms governing river–groundwater interactions in the Aksu River Basin. Rather than presenting these datasets in parallel, their combined interpretation reveals a coherent longitudinal exchange framework. Hydraulic gradients indicate an upstream losing reach, a midstream gaining reach, and a downstream losing reach. This pattern is independently supported by hydrochemical facies transitions, isotopic mixing proportions, and simulated exchange fluxes, demonstrating strong convergence among multiple lines of evidence. Minor discrepancies occur in transitional reaches, where isotopic signals suggest mixed recharge sources that cannot be fully resolved by hydraulic gradients alone.

Hydrochemical evolution provides mechanistic support for this pattern. Upstream waters are dominated by Ca^{2+}–HCO_3^- facies, reflecting rapid infiltration and carbonate weathering under short flow paths. In the midstream, increased SO_4^{2-} and Mg^{2+} concentrations indicate enhanced water–rock interaction and longer residence times associated with sustained groundwater discharge, suggesting a buffering function that stabilizes dry-season baseflow. Downstream Na^+ and Cl^- enrichment reflects evaporation concentration, irrigation return flow, and intensified abstraction, highlighting a shift from natural geochemical control in the upper basin to anthropogenic influence in the lower basin.

Isotopic evidence further constrains recharge sources. The similarity between $\delta^{18}O$–$\delta^{2}H$ signatures of downstream groundwater and river water, together with MixSIAR results indicating >60% river contribution, confirms river leakage as the dominant recharge source. In contrast, lighter isotopic signatures in the midstream suggest stronger contributions from snowmelt and local precipitation. Comparable spatial heterogeneity has been reported in other arid basins, including near-river exchange corridors in the Vredefort Dome and seasonal reversals in the Yiluo River Basin [72,73], indicating that such longitudinal variability represents a common response in arid river–groundwater interaction systems, though the magnitude of downstream leakage in the Aksu Basin reflects basin-specific anthropogenic forcing.

Numerical modeling provides dynamic support for these interpretations. The MIKE SHE model reproduces runoff with satisfactory performance (R^2 = 0.79–0.89), capturing

seasonal alternation between high-flow leakage and low-flow groundwater-supported baseflow. Reduced pumping scenarios demonstrate clear recovery of both river discharge and groundwater levels, underscoring the sensitivity of exchange processes to abstraction intensity. Similar anthropogenically induced shifts have been observed in the Chan and Shule River basins [74,75].

In addition to performance evaluation, parameter sensitivity can be inferred from calibration behavior and scenario responses. Although a formal global sensitivity analysis was not conducted, parameters requiring substantial adjustment during calibration—particularly riverbed hydraulic conductivity, horizontal hydraulic conductivity, and specific yield—exert dominant control on simulated exchange fluxes and groundwater dynamics. Riverbed conductance governs the magnitude and direction of leakage, hydraulic conductivity regulates spatial gradient redistribution, and specific yield controls groundwater-level responsiveness. The reduced-pumping scenario further confirms abstraction intensity as a first-order control factor. These results indicate that riverbed properties and pumping rates are the most influential parameters in the coupled system.

From a management perspective, the findings support strengthened conjunctive regulation of surface water and groundwater in the Aksu–Tarim system. Controlled river infiltration during wet seasons can enhance downstream storage, while excessive midstream pumping should be restricted to preserve baseflow. Withdrawal limits, zonal quotas, and improved irrigation efficiency are essential to mitigate salinization and sustain ecological functions.

These findings also provide practical implications for integrated water resources management (IWRM) in arid inland basins. The three-stage exchange framework identified in this study suggests that water management strategies should be spatially differentiated along the river corridor. In upstream losing reaches, maintaining adequate river discharge is necessary to sustain groundwater recharge and preserve hydrological connectivity. In midstream gaining reaches, where groundwater contributes significantly to river baseflow, stricter control of groundwater abstraction is required to prevent depletion of baseflow and associated ecological impacts. In downstream sections characterized by river leakage, coordinated regulation of irrigation return flows, drainage systems, and groundwater withdrawals is needed to reduce salinization risks and improve water-use efficiency. By explicitly incorporating river–groundwater connectivity into basin-scale allocation strategies, integrated water resources management can better balance agricultural water demand, ecological flow requirements, and long-term groundwater sustainability in the Tarim River Basin.

Despite the integrated framework, uncertainties remain due to limited observation density, potential parameter non-uniqueness, and simplified representation of irrigation processes. Future work should prioritize improved characterization of riverbed permeability, abstraction patterns, and high-resolution hydrogeological data to reduce uncertainty in coupled river–groundwater modeling.

Furthermore, the present model adopts a regional-scale conceptualization of the aquifer system based on available hydrogeological maps and groundwater observations, in which the quaternary alluvial deposits and hydraulically connected shallow aquifers are represented as a heterogeneous but isotropic hydrogeological unit. This simplification is appropriate for the basin-scale resolution and the primary objective of diagnosing dominant river–groundwater exchange patterns under intensive water use. However, subsurface heterogeneity may exhibit additional structural variability at finer lithological scales that cannot be explicitly resolved with the current data density and model resolution. Future investigations incorporating higher-resolution borehole lithological data, geophysical surveys, or facies-based conceptual frameworks could enable evaluation of alternative geo-

logical realizations and provide a more comprehensive assessment of structural uncertainty. Such developments would further strengthen confidence in simulated exchange fluxes and improve process-based understanding of river–groundwater interaction connectivity in arid alluvial systems.

In summary, the Aksu river–groundwater system is transitioning from a predominantly natural regime to a strongly human-modified system. The integrated analysis clarifies recharge–discharge mechanisms, reveals pronounced spatial heterogeneity, and demonstrates the high sensitivity of exchange processes to groundwater abstraction. Coordinated conjunctive management is therefore essential for long-term water sustainability in the Tarim Basin.

6. Conclusions

This study examined river–groundwater exchange mechanisms in the plain section of the Aksu River Basin through an integrated, multi-evidence framework combining hydraulic observations, hydrochemical indicators, stable isotopes, and distributed numerical modeling. Rather than relying on a single diagnostic approach, the study emphasizes cross-validation among independent lines of evidence to improve interpretative robustness at the basin scale.

(1) Spatial Pattern of River–Groundwater Exchange

All lines of evidence consistently indicate a three-stage longitudinal exchange pattern: upstream river recharge to groundwater, midstream groundwater discharge to the river, and renewed river infiltration to groundwater in the downstream reach.

Water-level measurements provide direct hydrodynamic evidence that hydraulic gradients primarily control recharge–discharge direction. Hydrochemical evolution shows a transition from low-mineralization HCO_3–Ca type groundwater in the upstream area toward SO_4^{2-}- and Cl^--enriched types downstream, reflecting progressive influence of evaporative concentration and salt dissolution processes. Stable isotope signatures (δ^2H and $\delta^{18}O$) support these findings, indicating dominant precipitation/snowmelt recharge upstream and increasing river-water contribution downstream. The MixSIAR analysis suggests that river-derived recharge exceeds 65% in the downstream section, whereas groundwater discharge dominates the midstream reach.

(2) Role of the Modeling Framework

The MIKE SHE model was employed to evaluate hydrological consistency and seasonal dynamics of river–groundwater exchange under varying flow conditions. The model reproduces seasonal bidirectional exchange behavior, with enhanced river infiltration during flood periods and groundwater-supported baseflow during dry seasons. Model performance during calibration and validation (R^2 = 0.84–0.91) indicates satisfactory representation of basin-scale hydrological processes.

Importantly, the modeling results are interpreted as supportive evidence within the broader multi-evidence framework, rather than as standalone quantitative proof of exchange flux magnitude.

(3) Spatial Heterogeneity and Temporal Dynamics

The results highlight pronounced spatial heterogeneity along the river corridor and clear seasonal variability in exchange behavior. Upstream–midstream–downstream contrasts are shaped by hydraulic gradients, sedimentary characteristics, evaporative intensity, and irrigation return flows, reflecting the complex interaction between natural processes and human activities in arid inland basins.

https://doi.org/10.3390/hydrology13030095

(4) Uncertainties and Limitations

Despite these findings, uncertainties remain. These include limited temporal observation periods, uneven spatial distribution of groundwater monitoring wells, and simplified representation of irrigation and drainage processes in the numerical model. These constraints may influence the precision of flux quantification but do not alter the identified large-scale spatial pattern of exchange. Future research incorporating longer monitoring records and refined irrigation-process representation would further improve model reliability.

(5) Implications for Integrated Water Resources Management

The identified exchange framework provides a scientific basis for integrated water resources management (IWRM) in the Tarim River Basin. Specifically, the results suggest that conjunctive regulation of surface water and groundwater is necessary to avoid overexploitation in gaining reaches.

Stricter control of groundwater abstraction is required in midstream areas where groundwater discharge sustains river baseflow. Promotion of water-saving irrigation practices can reduce downstream salinization risks and limit excessive river infiltration. Monitoring strategies should account for spatial heterogeneity in exchange dynamics. By linking hydrogeological mechanisms to management implications, this study contributes to sustainable water allocation, ecological flow maintenance, and long-term water security in arid inland river systems.

Supplementary Materials: The following supporting information can be downloaded at https://www.mdpi.com/article/10.3390/hydrology13030095/s1. Table S1: Hydrochemical parameters of river water and groundwater along the Aksu River cross-sections. Table S2: Proportions of hydrochemical element composition in river water and groundwater samples along the Aksu River cross-sections.

Author Contributions: J.B.: conceptualization, methodology, software, validation, formal analysis, investigation, data curation, writing—original draft preparation, visualization, project administration, funding acquisition. S.N.: conceptualization, methodology, validation, resources, writing—review and editing, supervision. Z.B.: validation, investigation, data curation, writing—review and editing. B.W.: writing—review and editing. C.Y.: writing—review and editing. All authors have read and agreed to the published version of the manuscript.

Funding: This research was funded by the 2022 Xinjiang Uygur Autonomous Region University Scientific Research Program (Category L), grant number XJEDU2022P052. The APC was also funded by this project.

Data Availability Statement: Publicly available datasets were analyzed in this study, as described in the manuscript. The processed datasets, field monitoring data, hydrochemical and stable isotope observations, and MIKE SHE model input/output data supporting the findings of this study are available from the corresponding author upon reasonable request.

Acknowledgments: This research was supported by the 2022 Xinjiang Uygur Autonomous Region University Scientific Research Program (Category L) [Grant number XJEDU2022P052]. Additionally, the authors would like to express their gratitude to the editor and anonymous reviewers for their constructive comments, which helped to significantly improve the quality of the manuscript.

Conflicts of Interest: The authors declare no conflict of interest.

References

1. Mi, L.; Xiao, H.; Zhu, W.; Li, J.; Xiao, S.; Li, L. Dynamic characteristics of groundwater level changes in the middle reaches of the Heihe River Basin from 1985 to 2013. *J. Glaciol. Geocryol.* **2015**, *37*, 461–469. [CrossRef]
2. Hu, R.J.; Fan, Z.L.; Wang, Y.J.; Jiang, F.Q. Groundwater resources and their characteristics in arid regions of northwest China. *J. Nat. Resour.* **2002**, 321–326.

3. Zhu, J.F.; Liu, Y.Y.; Zhang, S.A.; Zheng, H. Research progress on the interaction between surface water and groundwater. *China Environ. Sci.* **2017**, *37*, 3002–3010.
4. Huang, D.J.; Li, Y.P.; Cui, G.B.; Duan, Y.G.; Yao, L. Calculation method of basic ecological flow in river channels based on hydrology–hydraulics–habitat analysis. *Water Resour. Prot.* **2024**, *40*, 142–148. [CrossRef]
5. Zhang, W.C.; Shi, H.B.; Li, X.Y.; Li, H.; Zhou, H.; Wang, W. Study on soil water–groundwater dynamics and transformation relationship in a typical area of the Hetao Irrigation District. *Trans. Chin. Soc. Agric. Mach.* **2022**, *53*, 352–362. [CrossRef]
6. Lin, X.Y.; Liao, Z.S.; Qian, Y.P.; Su, X.S. Application of baseflow separation method in groundwater studies of the Yellow River Basin. *J. Jilin Univ. (Earth Sci. Ed.)* **2009**, *39*, 959–967. [CrossRef]
7. Harvey, J.W.; Newlin, J.T.; Krupa, S.L. Modeling decadal timescale interactions between surface water and ground water in the central Everglades, Florida, USA. *J. Hydrol.* **2006**, *320*, 400–420. [CrossRef]
8. Zhang, S.X.; Sun, Z.Y.; Pan, Y.X.; Li, X.; Pan, Z. Interaction between river water and groundwater in alpine regions based on temperature tracing: A case study of the upper Heihe River Basin. *Bull. Geol. Sci. Technol.* **2023**, *42*, 95–106. [CrossRef]
9. Lloyd, J.W. A review of aridity and groundwater. *Hydrol. Process.* **1986**, *1*, 63–78. [CrossRef]
10. Woessner, W.W. Stream and fluvial plain groundwater interactions: Rescaling hydrogeologic thought. *Groundwater* **2000**, *38*, 423–429. [CrossRef]
11. Liu, H.L.; Chen, X.; Bao, A.M.; Wang, L. Investigation of groundwater response to overland flow and topography using a coupled MIKE SHE/MIKE 11 modeling system for an arid watershed. *J. Hydrol.* **2007**, *347*, 448–459. [CrossRef]
12. Kim, N.W.; Chung, I.M.; Won, Y.S.; Arnold, J.G. Development and application of the integrated SWAT–MODFLOW model. *J. Hydrol.* **2008**, *356*, 1–16. [CrossRef]
13. Ehtiat, M.; Jamshid Mousavi, S.; Srinivasan, R. Groundwater modeling under variable operating conditions using SWAT, MODFLOW and MT3DMS: A catchment scale approach to water resources management. *Water Resour. Manag.* **2018**, *32*, 1631–1649. [CrossRef]
14. Guevara Ochoa, C.; Medina Sierra, A.; Vives, L.; Zimmermann, E.; Bailey, R. Spatio-temporal patterns of the interaction between groundwater and surface water in plains. *Hydrol. Process.* **2020**, *34*, 1371–1392. [CrossRef]
15. Zhou, C.H.; Yu, J.J. Review and prospect of hydrological geography research in China. *Acta Geogr. Sin.* **2023**, *78*, 1659–1665. [CrossRef]
16. Liu, C.M.; Liu, X.; Yu, J.J.; Yang, S.T.; Zhao, C.S.; Men, B.H.; Zhao, Z.L.; Wang, H.R. The rise of ecohydrology: A review of theoretical and practical issues. *J. Beijing Norm. Univ. (Nat. Sci.)* **2022**, *58*, 412–423. [CrossRef]
17. Zhang, H.B.; Zhi, T.; Wei, X.C.; Dang, C.H.; Xia, Y.; Gao, W.B. Simulation of runoff process and response to greening of the Loess Plateau in the middle Yellow River region based on SWAT–MODFLOW. *J. North China Univ. Water Resour. Electr. Power (Nat. Sci. Ed.)* **2020**, *41*, 1–10. [CrossRef]
18. Shu, L.C.; Yin, X.R.; Yuan, Y.J.; Lv, Y.; Lu, C.P.; Liu, B. Spatiotemporal variation of water exchange between river water and groundwater in a typical area of the Sanjiang Plain. *J. Hydraul. Eng.* **2021**, *52*, 1151–1162. [CrossRef]
19. Ren, J.W.; Hu, H.Z.; Tian, B.Y.; Yu, R.H.; Ren, R. Study on hyporheic exchange in a semi-arid grassland inland river: A case study of the Xilin River, Inner Mongolia. *China Rural Water Hydropower* **2021**, 46–52, 59.
20. Sun, J.; Wang, Y.X.; Yang, L.; Duan, L.M.; Chu, S.J.; Zhang, G.X.; Zhang, B.; Liu, T.X. Transformation relationship of precipitation, river water, and groundwater during the rainy season in the upper reaches of the Xilin River. *Environ. Sci.* **2023**, *44*, 6754–6766. [CrossRef]
21. Jin, X.; He, C.; Zhang, L.; Zhang, B. A modified groundwater module in SWAT for improved streamflow simulation in a large, arid endorheic river watershed in Northwest China. *Chin. Geogr. Sci.* **2018**, *28*, 47–60. [CrossRef]
22. Nian, Y.Y.; Li, X.; Zhou, J.; Zhou, J.; Hu, X.L. Impact of land use change on water resource allocation in the middle reaches of the Heihe River Basin in northwestern China. *J. Arid Land* **2013**, *6*, 273–286. [CrossRef]
23. Worqlul, A.W.; Ayana, E.K.; Yen, H.; Jeong, J.; MacAlister, C.; Taylor, R.; Gerik, T.J.; Steenhuis, T.S. Evaluating hydrologic responses to soil characteristics using SWAT model in a paired-watersheds in the Upper Blue Nile Basin. *Catena* **2018**, *163*, 332–341. [CrossRef]
24. Wang, Q.; Liu, R.; Men, C.; Guo, L. Application of genetic algorithm to land use optimization for non-point source pollution control based on CLUE-S and SWAT. *J. Hydrol.* **2018**, *560*, 86–96. [CrossRef]
25. Pang, J.; Bai, X.H.; Zhang, F.; Liu, X.F.; Zhang, B.L. Monthly runoff simulation in a typical area of the Loess Plateau based on the SWAT model. *Res. Soil Water Conserv.* **2015**, *22*, 111–115. [CrossRef]
26. Jin, X.; Jin, Y.X.; Yang, D.X. Impact of land use/cover change on hydrological processes based on LU–SWAT model: A case study of the upper Heihe River. *J. Irrig. Drain.* **2019**, *38*, 114–121. [CrossRef]
27. Song, Y.; Zhou, W.B.; Ma, Y.X.; Liu, B.Y.; Yan, Q.; Li, H. Analysis of the impact of precipitation, river runoff, and exploitation on the phreatic water flow field in Xi'an area. *Hydrogeol. Eng. Geol.* **2016**, *43*, 7–13. [CrossRef]
28. Jin, J.L.; Wang, G.Q.; Liu, C.S.; He, R.M.; Yan, X.L. Application of large-scale distributed hydrological model VIC to runoff simulation in the Jialing River Basin. *J. Water Resour. Water Eng.* **2012**, *23*, 55–58, 63.

29. Bai, M.; Mo, X.; Liu, S.; Hu, S. Contributions of climate change and vegetation greening to evapotranspiration trend in a typical hilly-gully basin on the Loess Plateau, China. *Sci. Total Environ.* **2019**, *657*, 325–339. [CrossRef]
30. Perkins, S.P.; Sophocleous, M. Development of a comprehensive watershed model applied to study stream yield under drought conditions. *Groundwater* **1999**, *37*, 418–426. [CrossRef]
31. Wang, X.H. Study on the Coupled Simulation and Regulation of Groundwater–Surface Water in the Sanjiang Plain. Ph.D. Thesis, Northeast Institute of Geography and Agroecology, Chinese Academy of Sciences, Changchun, China, 2015.
32. Carroll, R.W.H.; Deems, J.S.; Niswonger, R.; Schumer, R.; Williams, K.H. The importance of interflow to groundwater recharge in a snowmelt-dominated headwater basin. *Geophys. Res. Lett.* **2019**, *46*, 5899–5908. [CrossRef]
33. Sridhar, V.; Billah, M.M.; Hildreth, J.W. Coupled surface and groundwater hydrological modeling in a changing climate. *Groundwater* **2018**, *56*, 618–635. [CrossRef] [PubMed]
34. Kang, H.; Sridhar, V. Drought assessment with a surface–groundwater coupled model in the Chesapeake Bay watershed. *Environ. Model. Softw.* **2019**, *119*, 379–389. [CrossRef]
35. Wang, S.P.; Zhang, Z.Q.; Sun, G.; Strauss, P.; Guo, J.T.; Yao, A.K.; Tang, Y. Evaluation of hydrological impacts of land use and precipitation changes in the Chaohe River Basin based on the MIKE SHE model. *J. Ecol. Rural Environ.* **2012**, *28*, 320–325.
36. Han, Y.; Lu, W.X.; Li, F.P.; An, Y.K.; Zhang, J.W. Coupled simulation of surface water and groundwater quality in the Hun River Basin. *China Environ. Sci.* **2020**, *40*, 1677–1686. [CrossRef]
37. Liu, S.W.; Liu, H.L.; Wang, L. Development and application of the MIKE SHE model. *Hydrology* **2018**, *38*, 23–28.
38. Wu, Y.T.; Li, Z.J.; Qi, Z.Y.; Tong, R.X.; Yang, Z.J.; Huang, Y.C. Design flood calculation for data-scarce basins based on a hydrological model. *J. Hohai Univ. (Nat. Sci.)* **2023**, *51*, 1–8, 17.
39. Deng, C.; Sun, P.Y.; Yin, X.; Zou, J.C.; Wang, W.G. Runoff simulation in the upper Hanjiang River Basin based on a conceptual hydrological model coupled with a long short-term memory model. *J. Lake Sci.* **2025**, *37*, 279–292.
40. Gao, S.; Huang, Y.; Zhang, S.; Han, J.; Wang, G.; Zhang, M.; Lin, Q. Short-term runoff prediction with GRU and LSTM networks without requiring time step optimization during sample generation. *J. Hydrol.* **2020**, *589*, 125188. [CrossRef]
41. Geng, L.H.; Huang, Y.J.; Li, J.Q.; Chen, X.Y. Preliminary analysis of water resources characteristics in inland river basins of Northwest China. *Adv. Water Sci.* **2002**, *13*, 496–501.
42. Xia, J.; Shi, W. Study and prospect of water security issues in China under changing environments. *J. Hydraul. Eng.* **2016**, *47*, 292–301. [CrossRef]
43. Pei, H.W.; Wang, Y.F.; Shen, Y.J.; Ma, H.; Scanlon, B.R.; Liu, C.M. Impacts of agricultural development on groundwater resources in the U.S. High Plains and its implications. *Res. Agric. Mod.* **2016**, *37*, 166–173. [CrossRef]
44. Yang, Z.; Zhou, Y.; Wenninger, J.; Uhlenbrook, S.; Wang, X.; Wan, L. Groundwater and surface-water interactions and impacts of human activities in the Hailiutu catchment, northwest China. *Hydrogeol. J.* **2017**, *25*, 1341–1357. [CrossRef]
45. Zhang, B.; Hong, M.; Jia, Y.W.; Zhou, Z.H.; Lv, L.C. Study on distributed hydrological modeling based on MODFLOW in the middle and lower reaches of the Weihe River Basin. *Wetl. Sci.* **2009**, *7*, 148–154. [CrossRef]
46. Song, Q.F.; Chen, X.; Huang, R.C.; Zhang, Z.C. Simulation study on the impact of groundwater exploitation on runoff in agricultural irrigation areas. *China Rural Water Hydropower* **2017**, 103–106.
47. Zhang, J.Z.; Liu, J.X.; Ren, H.L. Analysis of the influence of underlying surface changes on runoff in the Guanting Reservoir area of the Yongding River Basin. *Haihe Water Resour.* **2016**, *6*, 7–10. [CrossRef]
48. Song, Z.F.; Zeng, J.J.; Jin, Y.Z.; Hu, X.Q.; Sun, D.Y.; Lu, S.C.; Zhang, Y.L. Distributed simulation of monthly runoff in the Shiyang River Basin based on SWAT model and SUFI-2 algorithm. *Bull. Soil Water Conserv.* **2016**, *36*, 172–177. [CrossRef]
49. Pan, Q.M.; Chang, X.H.; Jiang, X.H.; Liu, X.Y. Impact of groundwater utilization above Huayuankou on river runoff in the Yellow River. *People's Yellow River* **2014**, *36*, 55–57, 61. [CrossRef]
50. He, H.M.; Fu, X.F.; Cai, D.Y. Impact of riparian groundwater exploitation on river runoff in the lower reaches of the Yellow River. *People's Yellow River* **2008**, *30*, 59–61.
51. Meng, F.; Liu, T.; Huang, Y.; Luo, M.; Bao, A.; Hou, D. Quantitative detection and attribution of runoff variations in the Aksu River Basin. *Water* **2016**, *8*, 338. [CrossRef]
52. Chen, Y.N.; Xu, C.C.; Hao, X.M.; Li, W.H.; Chen, Y.P.; Zhu, C.G. Climate change in the Tarim River Basin over the past 50 years and its impact on runoff. *J. Glaciol. Geocryol.* **2008**, *30*, 921–929. [CrossRef]
53. Chen, Y.N.; Xu, Z.X. Possible impacts of global climate change on water resources in the Tarim River Basin, Xinjiang. *Sci. China Ser. D Earth Sci.* **2004**, *34*, 1047–1053.
54. Han, F.H.; Gao, F.; He, B.; Cao, Y.; Yao, X.C. Spatiotemporal trajectory and influencing factors of carbon emissions from land use in the Aksu River Basin from 1990 to 2020. *Environ. Sci.* **2024**, *45*, 3297–3307. [CrossRef]
55. Xu, L.; Yue, S.R.; Hu, X.F. Vegetation dynamics and driving mechanisms in the Aksu River Basin from 2000 to 2020. *Bull. Soil Water Conserv.* **2024**, *44*, 326–334. [CrossRef]
56. Gao, F.; Cao, Y.; Han, F.H.; He, B. Carbon emission trajectories and eco-environmental effects in the Aksu River Basin based on three types of spatial variations. *Environ. Sci.* **2024**, *45*, 6344–6353. [CrossRef]

57. D'Amore, F.; Scandiffio, G.; Panichi, C. Some observations on the chemical classification of ground waters. *Geothermics* **1983**, *12*, 141–148. [CrossRef]
58. Xie, J.; Liu, X.; Jasechko, S.; Berghuijs, W.R.; Wang, K.; Liu, C.; Reichstein, M.; Jung, M.; Koirala, S. Majority of global river flow sustained by groundwater. *Nat. Geosci.* **2024**, *17*, 770–777. [CrossRef]
59. Qiu, Y.T.; Chen, J.; Shu, L.C.; Yuan, Y.J.; Zhang, F.H.; Lu, C.P. Response of groundwater level to changes in precipitation and river water level in a typical area of the Sanjiang Plain. *South-to-North Water Transf. Water Sci. Technol. (Chin. Engl. Ed.)* **2022**, *20*, 1076–1083, 1127. [CrossRef]
60. Czuppon, G.; Tóth, A.; Fekete, E.; Fórizs, I.; Englender, A.; Kármán, K.; Dobosy, P.; Nyiri, G.; Madarász, T.; Szűcs, P. Stable isotope and hydrogeological measurements: Implications for transit time and mixing ratio in a riparian system of the Danube River. *J. Hydrol.* **2025**, *650*, 132412. [CrossRef]
61. Priya, G.; David, N.; Joseph, G.; Sweeney, C.; Vaughn, B.H. Demonstration of high-precision continuous measurements of water vapor isotopologues in laboratory and remote field deployments using wavelength-scanned cavity ring-down spectroscopy (WS-CRDS) technology. *Rapid Commun. Mass Spectrom.* **2009**, *23*, 2534–2542. [CrossRef]
62. Li, T.H.; Yin, P.F.; Lü, A.F.; Zhang, W.X.; Yin, J.Q.; Xiong, J.; Liu, Y.H. Spatiotemporal characteristics of vegetation climate productivity potential in the monsoon region of eastern China. *J. Northeast For. Univ.* **2023**, *51*, 62–69+91. [CrossRef]
63. Zhao, H.; Zhang, J.; James, R.T.; Laing, J. Application of MIKE SHE/MIKE 11 model to structural BMPs in S191 Basin, Florida. *J. Environ. Inform.* **2012**, *19*, 156–164. [CrossRef]
64. Thompson, J.R.; Sørenson, H.R.; Gavin, H.; Refsgaard, A. Application of the coupled MIKE SHE/MIKE 11 modelling system to a lowland wet grassland in southeast England. *J. Hydrol.* **2004**, *293*, 151–179. [CrossRef]
65. DHI Inc. *MIKE SHE User Manual Volume 2: Reference Guide*; DHI Inc.: Hørsholm, Denmark, 2008.
66. Li, J.; Jiao, S.L.; Liang, H.; Xiang, Z.; Xiang, S. Influence of precipitation time scale on runoff simulation in karst basins using the MIKE SHE distributed hydrological model: A case study of the Liudong River Basin in the Hongshui River system. *Carsologica Sin.* **2012**, *31*, 388–394.
67. Chen, G.; Li, W.J.; Lin, K.R. GIS-based flash flood risk assessment in Qingyuan City. *People's Zhujiang* **2017**, *38*, 55–59. [CrossRef]
68. Zhu, Q.A.; Zhang, W.C.; Zhao, D.Z. Study on spatial interpolation of daily precipitation for topographic elements based on PRISM and Thiessen polygons. *Sci. Geogr. Sin.* **2005**, 233–238.
69. Rujner, H.; Leonhardt, G.; Marsalek, J.; Viklander, M. High-resolution modelling of the grass swale response to runoff inflows with Mike SHE. *J. Hydrol.* **2018**, *562*, 411–422. [CrossRef]
70. Craig, H. Isotopic variations in meteoric waters. *Science* **1961**, *133*, 1702–1703. [CrossRef]
71. Shang, B.; Gao, J.; Chen, G.; Wu, Y. Stable isotopes in atmospheric water vapour: Patterns, mechanisms and perspectives. *Sci. China-Earth Sci.* **2024**, *67*, 3789–3813. [CrossRef]
72. Welgus, M.N.; Abiye, T.A. Surface water and groundwater interaction in the Vredefort Dome, South Africa: A stable isotope and multivariate statistical approach. *Environ. Monit. Assess.* **2022**, *194*, 672. [CrossRef]
73. Wang, X.; Jia, S.; Xu, Y.J.; Liu, Z.; Mao, B. Dual stable isotopes to rethink the watershed-scale spatiotemporal interaction between surface water and groundwater. *J. Environ. Manag.* **2024**, *351*, 119728. [CrossRef] [PubMed]
74. Yang, S.; Qian, H.; Xu, P.; Zhao, W.; Liu, Y.; Shen, Y.; Zang, Y.; Wang, Q.; Cao, Z. Hydrogeochemical genesis mechanism and interconversion processes of groundwater-surface water in the Chan River Basin, China: A new perspective from hydrochemistry and isotopes. *J. Environ. Sci.* **2025**, *157*, 890–907. [CrossRef] [PubMed]
75. Xie, C.; Liu, H.; Li, X.; Zhao, H.; Dong, X.; Ma, K.; Wang, N.; Zhao, L. Spatial characteristics of hydrochemistry and stable isotopes in river and groundwater, and runoff components in the Shule River Basin, Northeastern of Tibet Plateau. *J. Environ. Manag.* **2024**, *349*, 119512. [CrossRef] [PubMed]

Disclaimer/Publisher's Note: The statements, opinions and data contained in all publications are solely those of the individual author(s) and contributor(s) and not of MDPI and/or the editor(s). MDPI and/or the editor(s) disclaim responsibility for any injury to people or property resulting from any ideas, methods, instructions or products referred to in the content.